DESIGN OF A COMPUTER INTERFACE FOR AUTOMATIC FINITE ELEMENT ANALYSIS OF AN EXCAVATOR BOOM

A THESIS SUBMITTED TO
THE GRADUATE SCHOOL OF NATURAL AND APPLIED SCIENCES
OF
MIDDLE EAST TECHNICAL UNIVERSITY

BY

MEHMET YENER

IN PARTIAL FULFILLMENT OF THE REQUIREMENTS
FOR
THE DEGREE OF MASTER OF SCIENCE
IN
MECHANICAL ENGINEERING

MAY 2005

Approval of the Graduate School of Natural And Applied Sciences

Prof. Dr. Canan ÖZGEN

I certify that this thesis satisfies all the requirements as a thesis for the degree of Master of Science

Prof. Dr. Kemal İDER
Head of Department

This is to certify that we have read this thesis and that in our opinion it is fully adequate, in scope and quality, as a thesis for the degree of Master of Science

Prof. Dr. Eres SÖYLEMEZ
Supervisor

Examining Committee Members

Prof. Dr. Turgut TÜMER (METU,ME)

Prof. Dr. Eres SÖYLEMEZ (METU,ME)

Assoc. Prof. Suat KADIOĞLU (METU,ME)

Asst. Prof. Ergin TÖNÜK (METU,ME)

Prof. Dr. Yavuz YAMAN (METU,AEE)

I hereby declare that all information in this document has been obtained and presented in accordance with academic rules and ethical conduct. I also declare that, as required by these rules and conduct, I have fully cited and referenced all material and results that are not original to this work.

Name, Last name : Mehmet YENER

Signature :

ABSTRACT

DESIGN OF A COMPUTER INTERFACE FOR AUTOMATIC FINITE ELEMENT ANALYSIS OF AN EXCAVATOR BOOM

Yener, Mehmet
M.S, Department of Mechanical Engineering
Supervisor: Prof. Dr. Eres SÖYLEMEZ
May 2005, 95 pages

The aim of this study is to design a computer interface, which links the user to commercial Finite Element Analysis (FEA) program, MSC.Marc-Mentat to make automatic FE analysis of an excavator boom by using DELPHI as platform. Parametrization of boom geometry is done to add some flexibility to interface called OPTIBOOM. Parametric FE analysis of a boom shortens the design stages and helps to find the optimum design in terms of stresses and mass.

Keywords: Excavator boom, Finite Element Analysis, Parametric design, shape optimization.

ÖZ

EKSKAVATÖR BOMUNUN OTOMATİK SONLU ELEMANLAR ANALİZİNİ YAPABİLMEK İÇİN BİR BİLGİSAYAR ARAYÜZÜNÜN TASARLANMASI

Yener, Mehmet
Yüksek lisans, Makina Mühendisliği Bölümü
Tez Yöneticisi: Prof. Dr. Eres SÖYLEMEZ
Mayıs 2005, 95 sayfa

Bu çalışmada, kullanıcısı ile ticari sonlu elemanlar analizi programı MSC.Marc-Mentat arasında ekskavatör bomunun otomatik Sonlu elemanlar analizinin yapılabilmesi için bağlantı kuran, DELPHI platformu kullanılarak bir bilgisayar programı tasarlanmıştır. OPTIBOOM olarak adlandırılan arayüze esneklik eklemek için bomun parametrizasyonu yapılmıştır. Bomun parametrik sonlu elemanlar analizi, tasarım aşamasını kısaltır ve optimum gerilme ve kütle için en uygun tasarımın bulunmasına yardımcı olur.

Anahtar kelimeler: Ekskavatör bomu, Sonlu elemanlar analizi, Parametric tasarım, Şekil optimizasyonu.

ACKNOWLEDGMENTS

The author expresses sincere appreciation to Prof. Dr. Eres SÖYLEMEZ for his guidance and insight throughout the research

The author would also like to thank his office mates Levent İPEK, Ayhun ÜNAL and Koray ÖZBAY for their suggestions and helps in computer programming.

This study was supported by Hidromek Ltd.

TABLE OF CONTENTS

pa

LIST OF TABLES

TABLE

LIST OF FIGURES

FIGURE

CHAPTER 1

INTRODUCTION

Excavator (Figure 1.1) is a mobile machine that is moved by means of either crawler track or rubber-tired undercarriage [29]. It has a specific feature that, its upper structure is capable of full rotation, and thus it has a wide working range. Excavator digs, elevates, swings and dumps material by the action of its mechanism, which consists of boom, arm, bucket and hydraulic cylinders. Bucket is used for trenching, in the placement of pipe and other under-ground utilities, digging basements or water retention ponds, maintaining slopes and mass excavation. Due to severe working conditions, excavator parts are subject to corrosive effects and high loads. The excavator mechanism must work reliably under unpredictable working conditions.

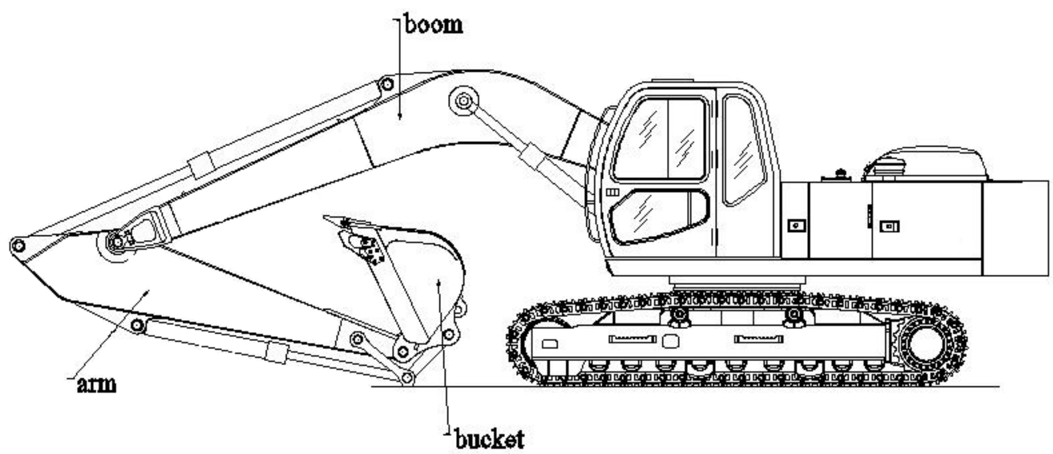

Figure 1.1: HMK 220 LC Excavator general view

Poor strength properties of the excavator parts like boom, arm and chassis limit the life expectancy of the excavator. Therefore, excavator parts must be strong enough to cope with caustic working conditions of the excavator. It can be concluded that, strength analysis is an important step in the design of excavator parts.

Finite Element Analysis (FEA) is the most powerful technique in strength calculations of the structures working under known load and boundary conditions. One can determine the critical loading conditions of the excavator by performing static force analysis of the mechanism involved for different piston displacements. The boundary conditions for strength analysis will be determined according to the results of static force analysis. In general, computer aided drawing (CAD) model of the parts to be analyzed must be prepared prior to the FEA. Preparation of the CAD model can be done either using a commercial FEA program or using a separate commercial program, which is specialized for CAD. Although most of the commercial FEA programs have CAD feature, they are not as good as the programs that are specialized in CAD and CAD programs that have FEA feature have limited capabilities. Therefore, CAD modeling and FE analysis are performed using two different programs. Preparation of the CAD model and performing FE analysis take considerable amount of time and needs experienced user.

The aim of this study is to design a computer interface, which will be used in the automatization of FEA of an excavator boom in a commercial FEA program. This study is mainly focused on the strength analysis of the boom. It is not concerned with the strength analysis of the arm, the bucket and the chassis of an excavator. Starting from the user specified shape parameters; the interface designed will compute all the necessary data that is required for the strength analysis in a commercial FEA program. By using this interface, it will also be possible to change the position of the boom and boundary conditions at which the analysis is performed. Using the software developed, finite element analysis of an excavator boom will be simplified and the need to use a separate commercial CAD program will be eliminated.

The excavator analyzed in the present study is a HMK 220LC model excavator, which is currently being manufactured by HIDROMEK Ltd.

At the beginning of this work, kinematic analysis and static force analysis of this excavator mechanism will be carried out to determine the digging force of the excavator at different mechanism positions. Since the motion of an excavator boom is slow, inertial effects due to the motion of the boom and the arm is not considered.

In the second part of the thesis, after the force analysis, a finite element method that will be used in the strength analysis of the HMK 220LC model excavator boom will be determined. Finally a computer interface that supplies all required information to commercial FEA program (MSC.Marc-Mentat) for performing finite element analysis of an excavator boom will be designed. And this interface will be used in the design of HMK 220LC.

CHAPTER 2

LITERATURE SURVEY

Structural optimization for strength is a popular subject in modern engineering design. It has been widely used to obtain an optimum strength/material mass ratio for structures under specified load conditions.

In general there are 3 types of structural optimization techniques [6]: sizing, geometrical and topology optimization. In sizing and geometrical optimization, topology of the structure does not change during the optimization process. In these techniques, designer searches the best solution among the possible geometries, which can be obtained by changing the shape parameters. These methods do not guarantee that the structure obtained is the best solution. Changing the initial topology may give better results. In topology optimization, best topology for the given problem is also searched.

Xie and Steven [7] have developed an approach called as ESO (evolutionary structural optimization) based on topology optimization. Main idea behind ESO is removal of inactive materials (elements) from the design domain after performing FE analysis. Element removal process is mainly based on the von Mises stress in the elements. The authors define a rejection criterion that is specific to each application. Element removal process continues until the rejection criterion is reached.

Pasi Tanskanen [6] states that, ESO tends to produce truss-like topologies even when applied to plane stress element models because; if a significant part of the design domain is subjected to uniaxial stresses, it follows that the objective function cannot reach the minimum until all the elements are subjected to a constant strain energy density value.

R. Das, R. Jones and Y.M. Xie [8] state that, The ESO algorithm employs the initial finite element model throughout the optimization process. Hence it alleviates problems associated with remeshing.

The second optimization technique is geometrical optimisation. Parametric definition of the geometry leads to the redesign of the initial shape by changing these parameters. H. Ugail and M.J. Wilson [1] state in their work that; the basic approach in parametric design is to develop a generic description of an object or a class of objects in which the shape is controlled by the values of a set of design variables or parameters. A new design, created for a particular application, is obtained from this generic template by selecting particular values for the design parameters. By using parametrization, optimum solution can be searched among the possible shapes that are created by changing the parameters.

Joong Jae Kim and Heon Young Kim [3] have developed an optimization code to determine the shape to meet the stiffness requirement of engine mount, coupled with a commercial nonlinear finite element program. A bush type engine mount being used in a passenger car has been chosen for the application model. They have modeled the engine mount by using 6 dimensional parameters and they found the optimum solution by selecting specific values for the 6 different geometrical parameters.

Wang [4] worked on the optimization of a metal container. He parameterized the metal container by 4 parameters and performed implicit quasi-static and linearized buckling analyses. His aim was to minimize the material usage while satisfying both the axial load and the paneling requirements.

Hardee et al. [5] Presented a CAD-based design sensitivity analysis (DSA) and optimization method using Pro/ENGINEER for shape design of structural components in their work. Their idea is that, variable dimensions may be used as the design variables for the shape optimization of the design, the CAD model may then be used directly in the design optimization process. They applied their method to a turbine blade. The shape of the shank and the position of the dovetail were parameterized to modify and improve the structural performance of the blade.

D.Holm et al. [2] Perform optimization by using the OASIS-ALADDIN software. One of the applications is the weight minimization with stress constraints of an axle housing to a wheel loader. They have represented the axle housing with 33 shape variables, which represent the interior shape, shape of the stiffeners and the plate. Another optimization work is on the minimization of stress intensity factors, in order to maximize fatigue life of a disc in an excavator boom (Figure 2.1). In this study, they model the boom and arm and they create sub-model of the middle disc, the disc shape is represented by means of shape parameters that are nodal coordinates of certain points (Figure 2.2). By changing nodal coordinates, the disc shape can also be changed.

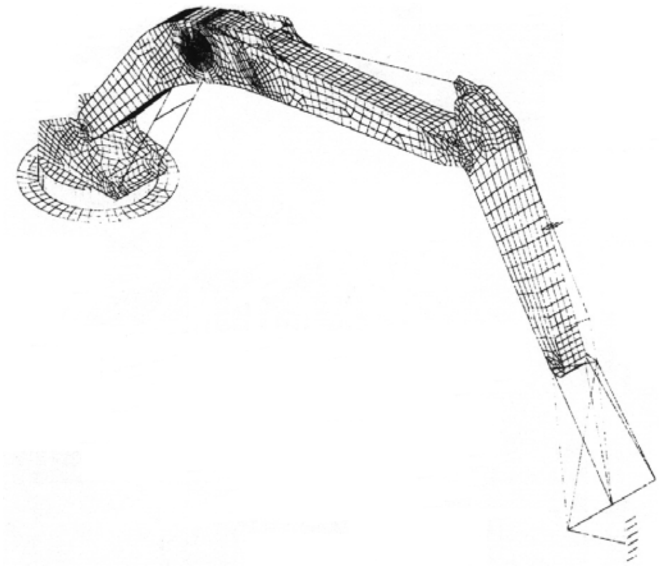

Figure 2.1: Excavator FEA model given in [2]

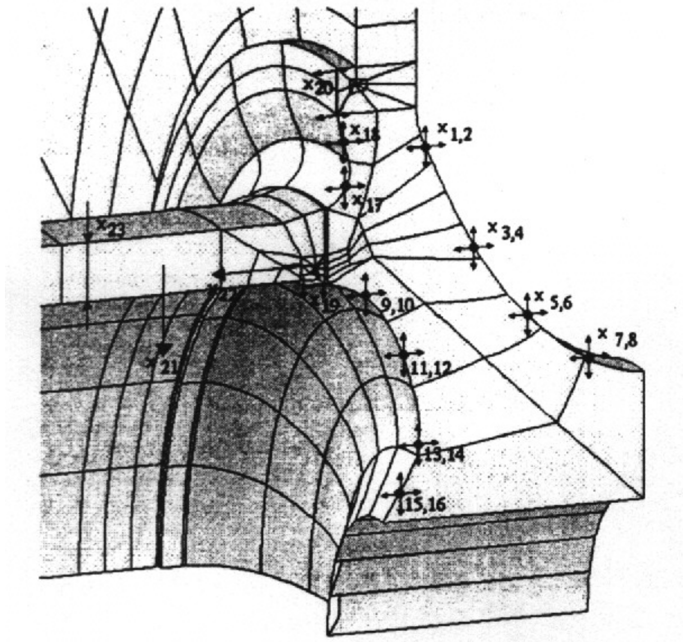

Figure 2.2: Sub-model of the joint disc in [2]

In the literature, there are also studies on the analysis and design of excavator booms. John E. Pearson et al. [16] worked on the experimental stress analysis of an excavator boom to develop a fatigue monitoring system. They installed strain gauges at several locations where crack had previously occurred and to some other locations sufficient to obtain an understanding of the strains throughout the structure. They monitored the static and dynamic loading data to develop a structural maintenance program.

Lee et al. [17] studied the design of a pneumatic excavator boom (Figure 2.3) for educational purposes. Pro/Engineer is used to construct the parametric solid model for finite element analysis.

Martinsson in his doctoral thesis [18], worked on the weldments in complex structures. This study had the aim of improving lead-time, accuracy and material utilization of fatigue-loaded complex welded structures such as construction machinery, busses, forest machines, robots, cranes and ship structures. The main objective in this thesis is to develop novel procedures to extract design data from FEA of complex welded structures, to achieve a better understanding of the limits of the different fatigue design methods and to investigate the infuence of fatigue strengh due to the weld quality. Based on the conclusions of the investigations, an automatic 3D FEA based LEFM program was developed by Martinsson.

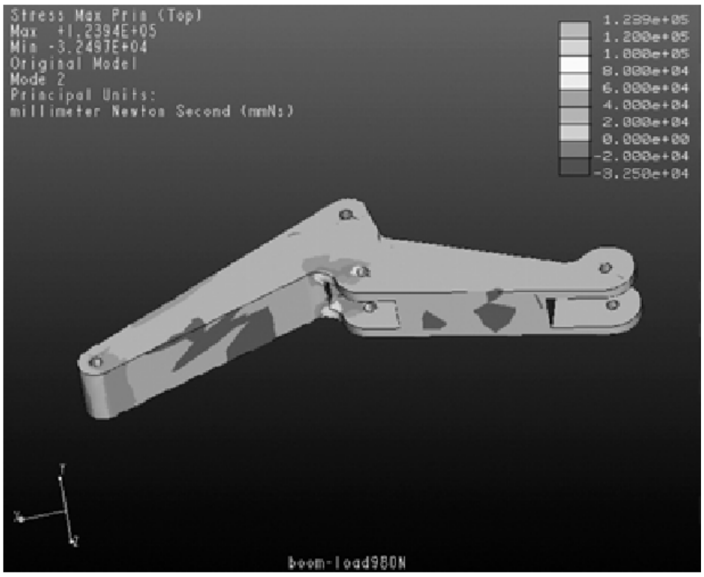

Figure 2.3: FEA of the boom designed by Lee, Chang and Lin [17]

Lee and Kwak [19] worked on the structural optimization by using Taguchi method [30]. The Taguchi method is applied iteratively to update the values of design variables. In this work, the authors implement this method into a parametric CAD platform with commercial FEA codes. One of their case studies is, the optimization of an excavator boom. They model the excavator boom with 1816 quadrilateral and 179 triangular elements. Maximum excavating force exerted on the bucket is found to be 123.4 kN and this value is used in the finite element model. Using 4 geometric and 9 thickness parameters, von Mises stresses in the structure and material usage is reduced. Optimum solution is computed after 22 iterations and 639 FEA runs. The parameters used in this work and shapes of the initial and optimized models are shown in Figure 2.4.

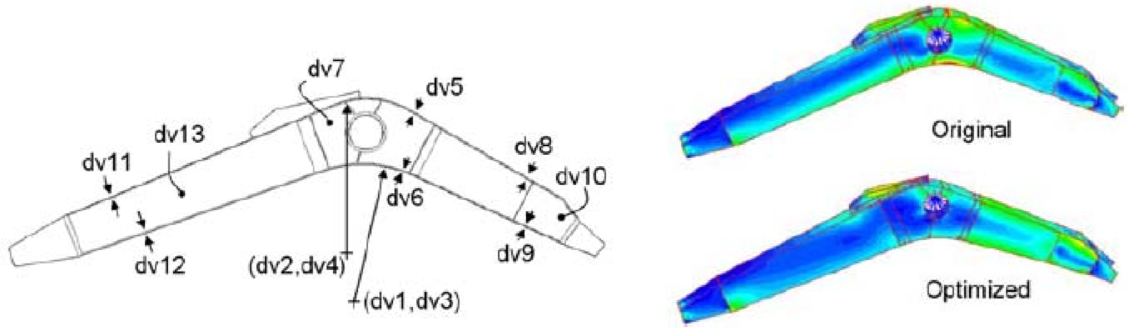

Figure 2.4: Boom parameters and stress distribution on the booms in Lee's work [19]

CHAPTER 3

KINEMATIC ANALYSIS AND DIGGING FORCE CALCULATION OF AN EXCAVATOR

Excavator is a three-degree of freedom system, consisting of three different mechanisms each of which can be controlled independently (Figure 3.1). The first mechanism is for the rotation of the boom, which is actuated by boom cylinders thus forming an inverted slider-crank mechanism relative to the frame. The second mechanism is for the rotation of the arm (dipper stick) relative to the boom actuated by the arm cylinders. This is also an inverted slider crank mechanism. The third mechanism is for the rotation of the bucket. Since a large bucket oscillation is required, the mechanism used is a series combination of a four-bar and an inverted slider-crank mechanism, which forms a 6-link mechanism relative to the arm.

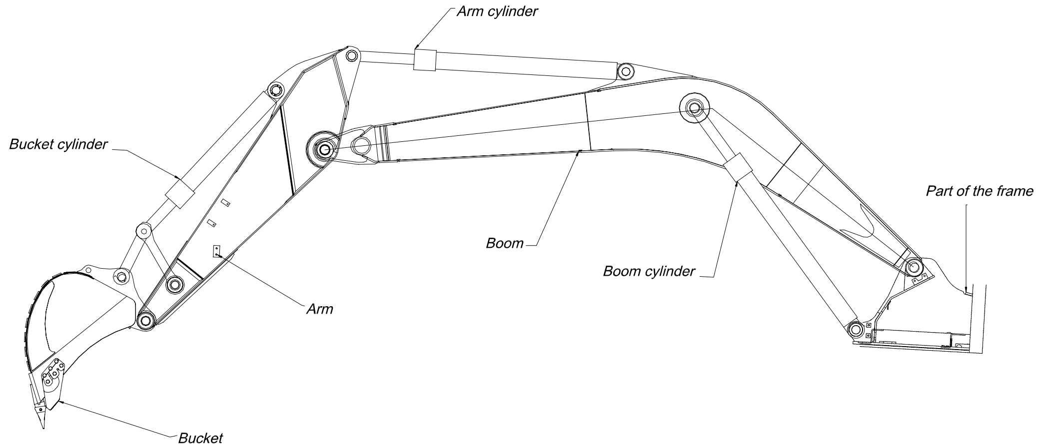

Figure 3.1: Excavator mechanism

3.1 Position analysis of the mechanism

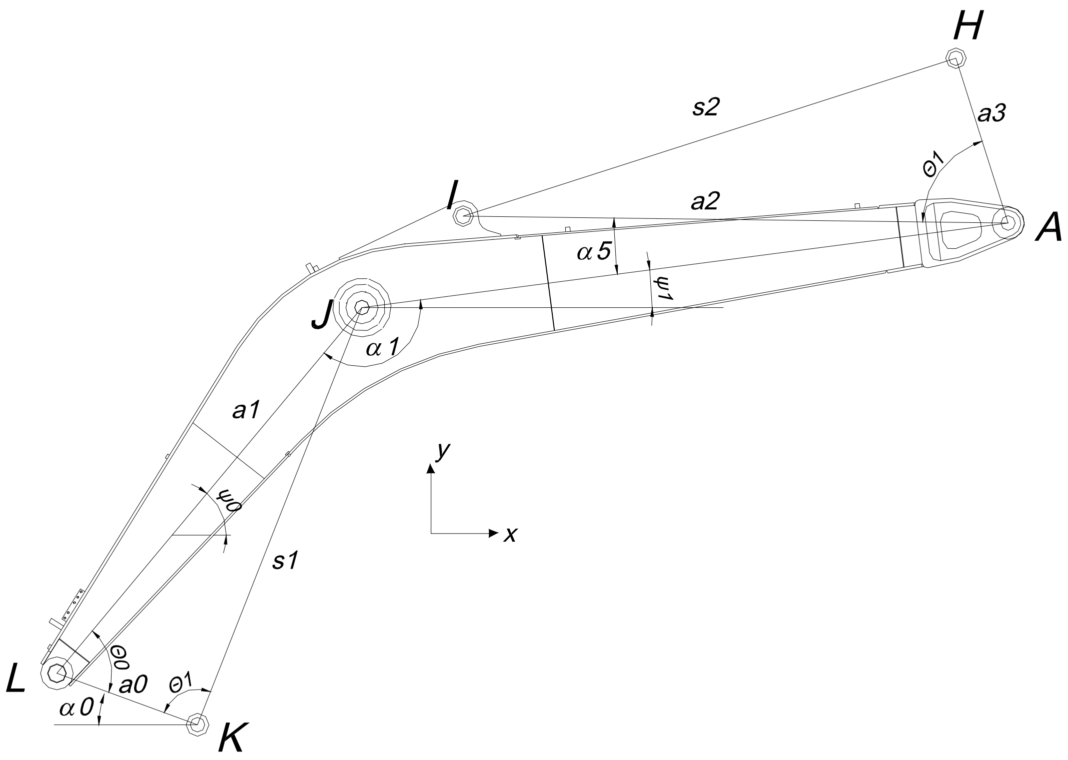

Figure 3.2: Mechanism parameters in boom

KJ and IH are the hydraulic piston-cylinder positions having lengths s_1 and s_2 respectively (Figure 3.2). Points L and K are pivot points of the boom and boom cylinder on the chassis respectively.

Boom position with respect to *x*-axis can be defined by the angle Ψ_0 (Figure 3.2) and calculated as;

$$\Theta_0 = \arccos\left(\frac{a_0^{\;2} + a_1^{\;2} - s_1^{\;2}}{2.a_0.a_1}\right)$$
$$\Psi_0 = \Theta_0 - \alpha_0 \tag{3.1}$$

Position of the arm with respect to *x*-axis (Ψ_2) can found as (Figure 3.3);

$$\Theta_1 = \arccos\left(\frac{a_2^{\;2} + a_3^{\;2} - s_2^{\;2}}{2.a_2.a_3}\right)$$
$$\Psi_1 = \Psi_0 + \alpha_1 - \pi \tag{3.2}$$
$$\Psi_2 = \pi + \Psi_1 - \alpha_5 - \Theta_1$$

Bucket is the output link of the four-bar mechanism CEFD (Figure 3.3). The piston-cylinder placed in between points GE actuates this mechanism. To find the position of bucket, position of crank (CE) must be defined first. Crank position (Ψ_{10}) and bucket position can be calculated from the equations:

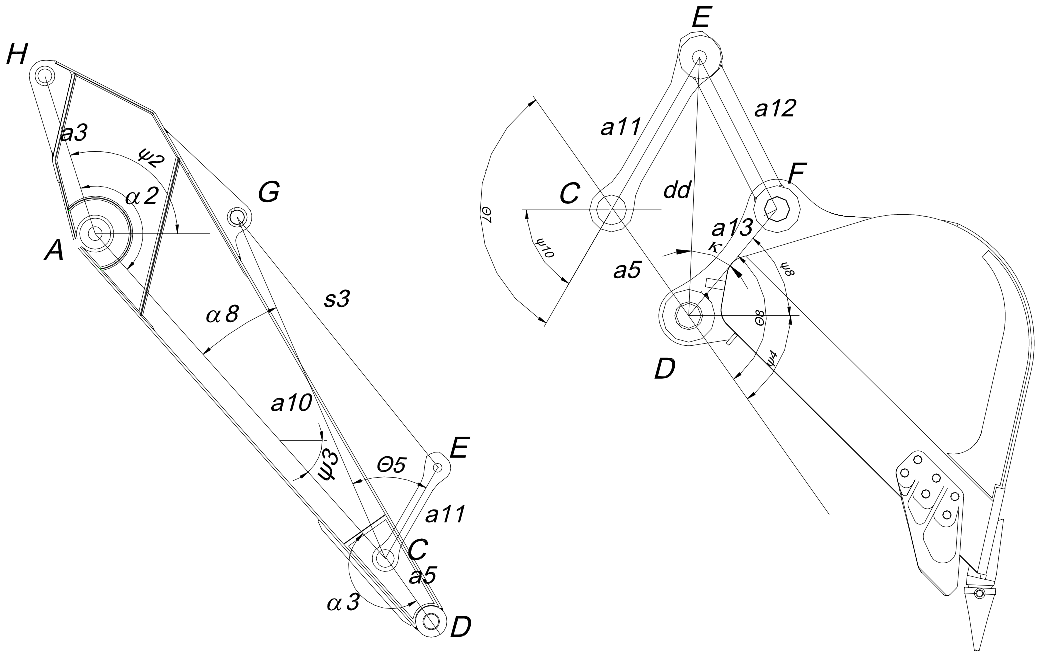

Figure 3.3: Mechanism parameters in arm and bucket

$$\Theta_5 = \arccos(\frac{a_{10}^2 + a_{11}^2 - s_3^2}{2.a_{10}.a_{11}})$$
$$\Psi_3 = \Psi_2 - \alpha_2 \tag{3.3}$$
$$\Psi_{10} = \pi + \Psi_3 - \alpha_8 - \Theta_5$$

$$xd = -a_5 + a_{11}.\cos\Theta_7$$
$$yd = a_{11}.\sin\Theta_7$$
$$\psi = a\tan 2(\frac{yd}{xd})$$
$$dd = \sqrt{xd^2 + yd^2}$$
$$\kappa = \arccos(\frac{a_{13}^2 + dd^2 - a_{12}^2}{2.a_{13}.dd}) \tag{3.4}$$
$$\Theta_8 = \psi - \kappa$$
$$\Theta_7 = 2\pi - \alpha_3 - \alpha_8 - \Theta_5$$
$$\Psi_4 = \Psi_3 - \pi + \alpha_3$$
$$\Psi_8 = \Psi_4 + \Theta_8$$

When the link dimensions and the piston displacement (s_3) is given, the above equations can be used to determine the position of links CE, EF and FD (Bucket) relative to the arm. Since the position of the boom and the arm can be determined from equations 3.1 and 3.2 respectively, the position of all the rigid bodies that form the excavator can be evaluated when the three piston displacements (s_1, s_2, s_3) and the link lengths are given.

3.2 Digging force calculations

Hydraulic cylinders apply force to boom, arm and the bucket to actuate the mechanism. Depending on the mechanism position, working pressure and diameter of the hydraulic cylinders, the amount of excavation force changes. In practice, boom cylinders are used for adjusting the bucket position not for digging. Arm cylinder and bucket cylinder are used for excavating. Thus, calculation of digging force must be carried out separately when arm cylinder or bucket cylinder is the active cylinder.

3.2.1 Force calculation when arm cylinder is active

Force created by the cylinder can be found by using its piston diameter and working pressure.

$$F_{s_2} = P.\pi \frac{D^2}{4}$$

where

P is the working pressure of the cylinder and *D* is the diameter.

Moment created on the arm is:

$$M = a_3.\sin\Theta_3.F_{s_2} \tag{3.5}$$

Excavation force and the application angle can be found by using parameters in Figure 3.4 as

$$\Theta_3 = \arccos\left(\frac{{s_2}^2 + {a_3}^2 - {a_2}^2}{2.s_2.a_3}\right)$$
$$h = \sqrt{xh^2 + yh^2}$$
$$xh = a_4.\cos\Psi_3 + a_5.\cos\Psi_4 + a_{14}.\cos(\alpha_9 - \Psi_8)$$
$$yh = a_4.\sin\Psi_3 + a_5.\sin\Psi_4 + a_{14}.\sin(\alpha_9 - \Psi_8)$$

$$F = \frac{M}{h}$$
$$z = \sqrt{{a_4}^2 + {a_5}^2 - 2.a_5.a_4.\cos\alpha_3}$$

$$\Theta_{20} = \arccos\left(\frac{a_{14}{}^{2} + h^{2} - z^{2}}{2.a_{14}.h}\right)$$
$$\Theta_{F} = \frac{\pi}{2} + \Theta_{20} + \Psi_{8} - \alpha_{9} \qquad (3.6)$$

where

h is the distance from point A to Point B (Figure 3.3)

F is the excavation force

Z is the distance from point A to point D

Θ_{20} is the angle ABD

Θ_{F} is the application angle of excavation force from x-axis

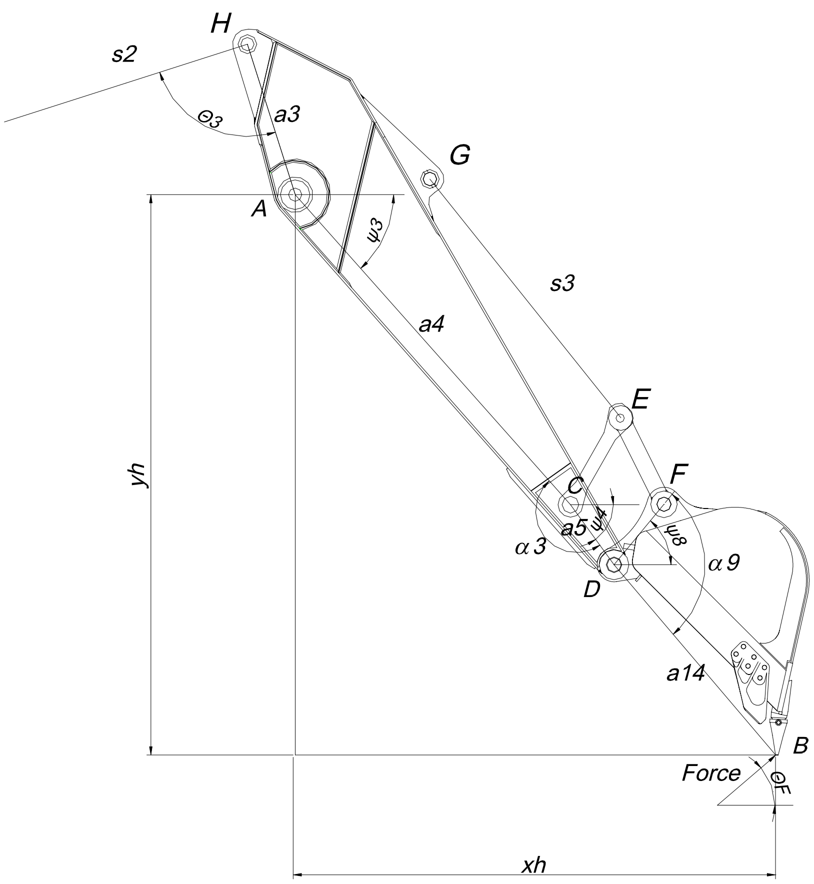

Figure 3.4: Force calculation when arm cylinder is the active cylinder

3.2.2 Force calculation when bucket cylinder is active

Moment created on the crank by bucket cylinder is:

$$M = a_{11}.\sin\Theta_6.P.\pi\frac{D^2}{4}$$

where;

P is the working pressure of bucket cylinder and D is the diameter.

From Figure 3.5, the excavation force and its application angle can be written as;

$$F = \frac{M}{a_{14}}$$
$$\Theta_F = \frac{\pi}{2} + \Psi_8 - \alpha_9 \qquad (3.7)$$

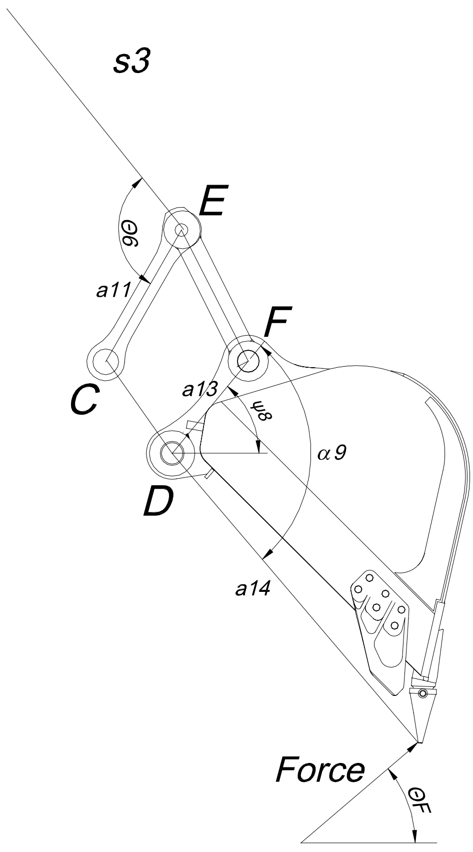

Figure 3.5: Force calculation when bucket cylinder is the active cylinder

3.3 Determination of maximum digging force

During motion of the excavator mechanism, excavation force and its angle of application changes. Digging force calculation is defined by SAE J1179 (Hydraulic Excavator and Backhoe digging forces) standard [28]. This standard defines the maximum digging force as: ‘*The maximum digging forces are the digging forces that can be exerted at the outermost cutting point. These forces are calculated by applying working circuit pressure to the cylinder(s) providing the digging force without exceeding holding circuit pressure in any other circuit. Weight of the components and friction are to be excluded from these force calculations.’* Digging forces must be calculated for the active cylinder(s). SAE J1179 shows the way of calculating maximum digging forces for the bucket and the arm cylinder not for boom cylinder. Standard states that, ‘*The maximum bucket tangential force, ‘V’, (Figure3.6) is the digging force generated by the bucket cylinder(s) and tangent to the arc of radius ‘C’. The bucket shall be positioned to obtain the maximum output moment from the bucket cylinder(s) and connecting linkage.’* Maximum arm force is also defined as ‘ *The maximum arm/dipperstickforce, ‘W’ (Figure 3.7) is the digging force generated by the arm/dipperstick cylinder(s) and tangent to the arc of radius ‘B’. The arm/dipperstick shall be positioned to obtain the maximum output moment from the arm/dipperstick cylinder(s) and the bucket positioned as in the case of maximum bucket tangential force.’*

Boom cylinders are not used for digging. Therefore, digging force calculation when boom cylinders are active is not considered in this study.

According to the SAE J1179, maximum digging forces of an excavator can be calculated by using the equations given by 3.2.1 and 3.2.2 and maximum digging force position can also be found. The standard and the equations obtained are applicable to any excavator.

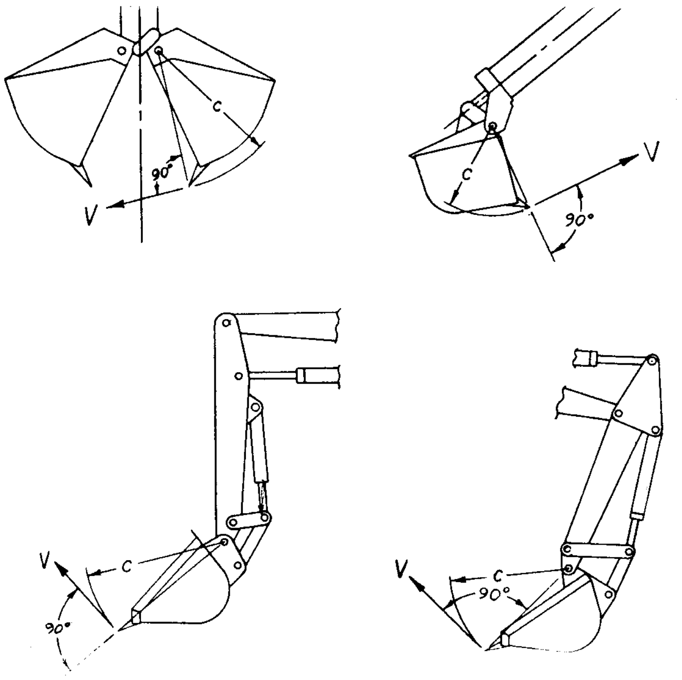

Figure 3.6: Maximum bucket tangential force [28]

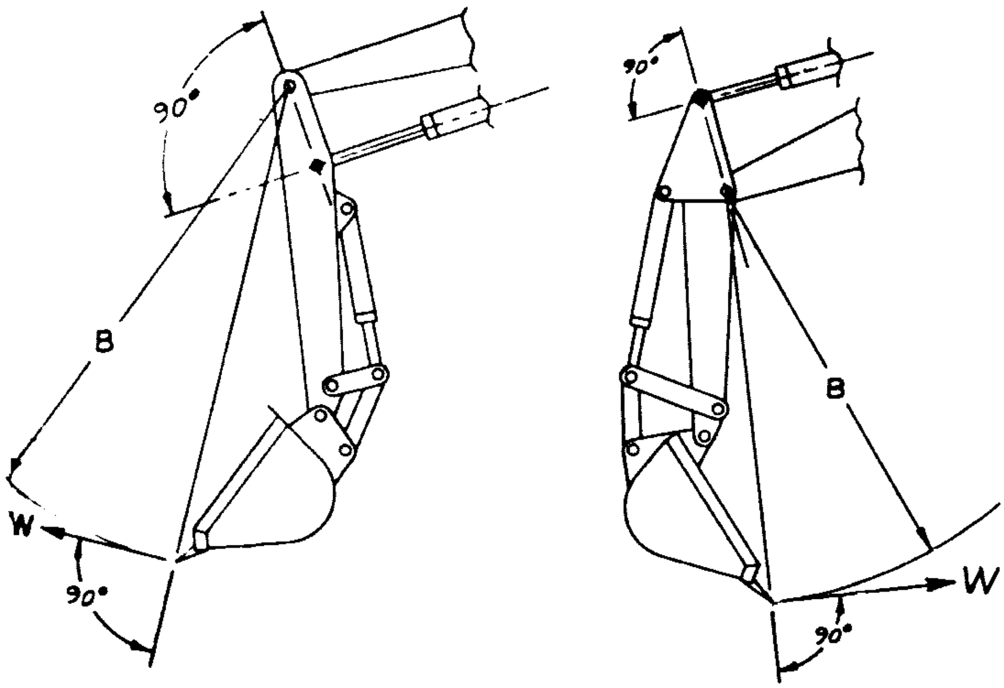

Figure 3.7: Maximum arm/dipperstick force [28]

CHAPTER 4

FINITE ELEMENT ANALYSIS OF HMK 220LC EXCAVATOR BOOM

In this chapter, finite element analysis of the HMK 220LC boom produced by Hidromek is performed by using MSC.Marc. Assumptions in the analysis, determination of boundary conditions, convergence check and verification of the analysis results by experimental stress analysis are also described.

4.1 Assumptions

1- It is assumed that material behavior is linear elastic and strains are small. Therefore, linear elastic analysis will be carried out.
2- Except the middle mechanism joint and rear bushings, sheet metal parts of the boom will be modeled using quadrilateral thick shell elements. Joints (Figure 4.1) will be modeled using tetrahedral solid elements. No special tying will be used in shell to solid transition. Solid and shell elements will be attached directly from their nodes.
3- Not only boom, but also arm, bucket and connecting linkage will also be modeled. However, only the boom will be realistically modeled. Hydraulic cylinders, arm, bucket and connecting linkage will be modeled using beam elements (Figure 4.2). Boom, arm, bucket, connecting linkage and hydraulic cylinders will be connected by using special tying links from the

joints. These tying links in MSC.Marc, equalize all degrees of freedom of two nodes except joint rotation direction.

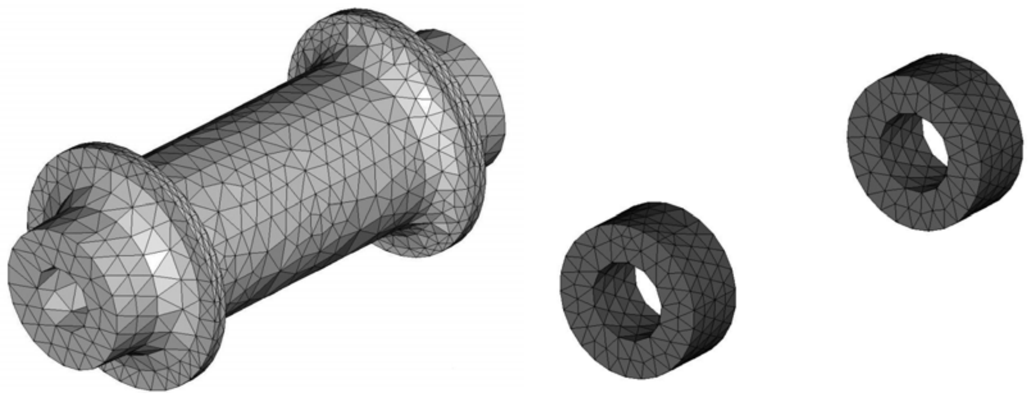

Figure 4.1: Mesh of middle joint and rear bushings

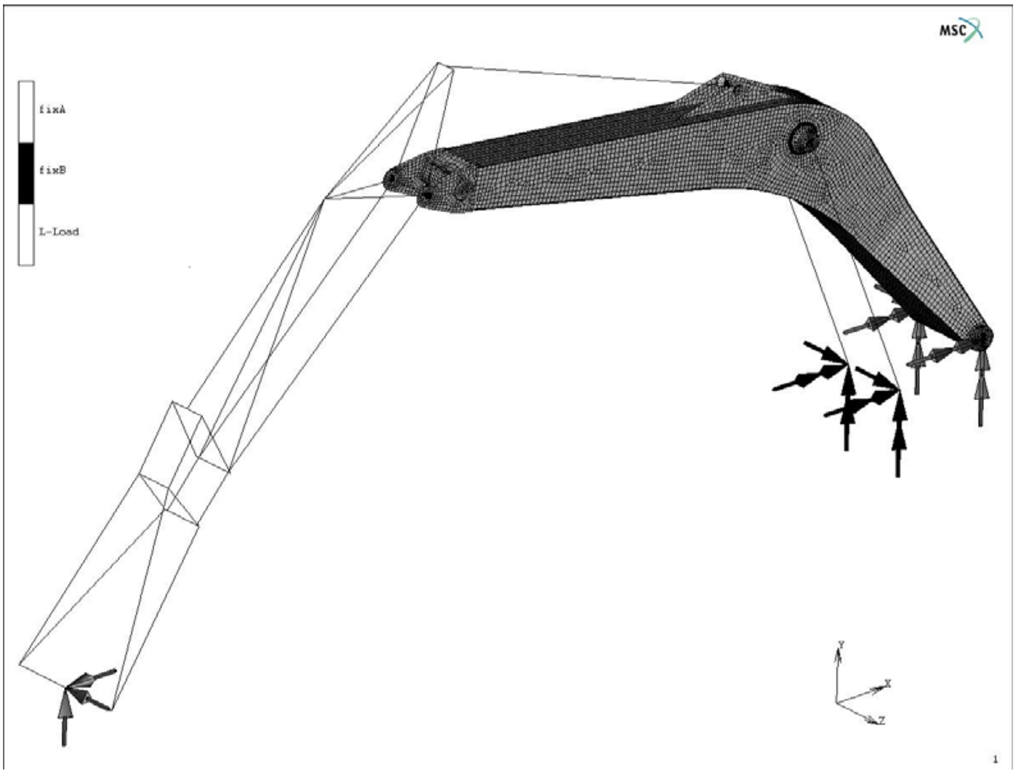

Figure 4.2: FEA model of excavator mechanism

4.2 Boundary Conditions

At the maximum digging force position, excavator mechanism is subjected to maximum forces. Therefore, finite element analysis must be performed under the maximum digging force value and maximum digging force position. By using equations obtained in Ch 3 and SAE J1179 [28], maximum digging force position and value of digging forces when bucket and arm cylinders are active, can be calculated for HMK 220LC. Figure 4.3 and Figure 4.4 shows the changes in the digging force for bucket and arm cylinder of HMK 220LC respectively. In these figures s_3 is the length of the bucket cylinder and s_2 is the length of the arm cylinder.

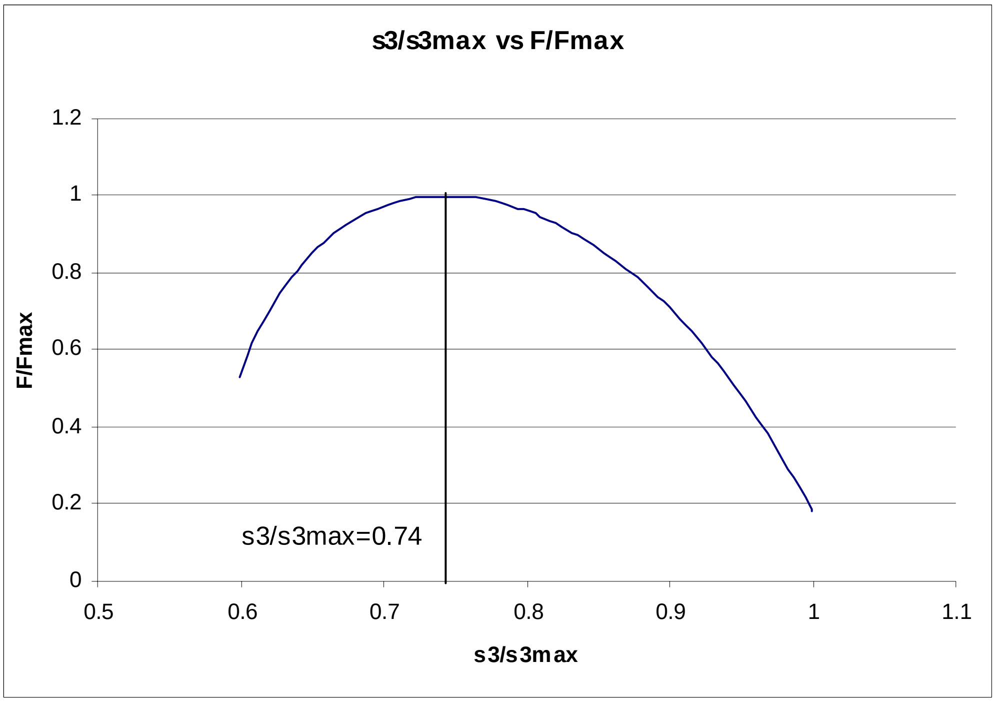

Figure 4.3: s_3/s_{3max} vs F/F_{max}

As stated in Ch 3, SAE J1179 does not specify the length of the boom cylinder. However length of boom cylinder can be selected to bring the mechanism to proper digging position where the tip of the bucket touches the ground.

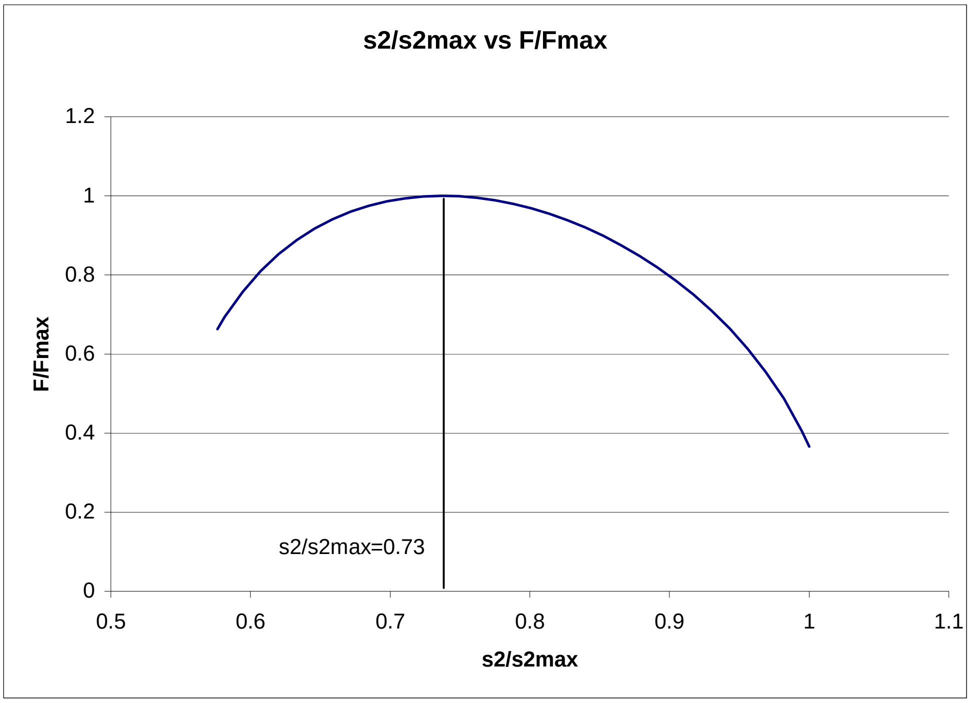

Figure 4.4: s_2/s_{2max} vs F/F_{max}

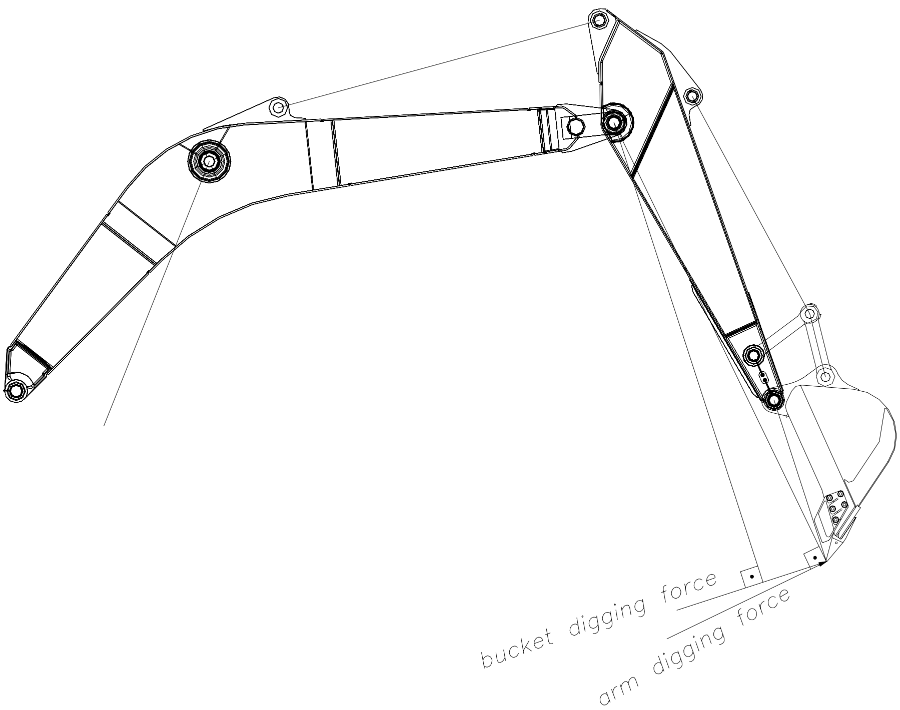

Figure 4.5: Maximum digging force directions for HMK 220 LC

For HMK 220LC, digging force created by bucket cylinder is greater than the digging force of arm cylinder. However bucket digging force creates less moment on the boom than that of the arm digging force since, perpendicular distance from the direction of bucket digging force to boom front joint is small (Figure 4.5). Therefore, arm digging force is more critical for boom when strength calculation is considered.

Upper part of an excavator is capable of full rotation about the center of the chassis by means of a hydraulic system. This system applies a moment *'M'* as Figure 4.6 to upper part of an excavator. This moment induces a force *'F'* at the tip of the bucket. Therefore, in finite element analysis, arm digging force and bucket lateral force will be applied as forces at the tip of the bucket (Figure 4.2).

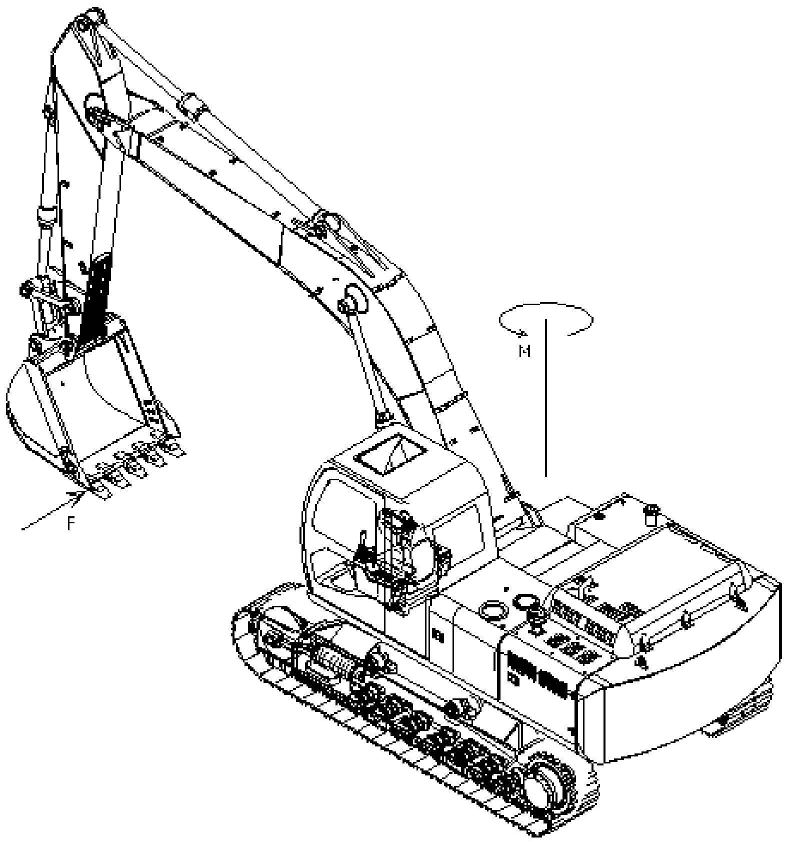

Figure 4.6: Lateral force on the bucket

In finite element analysis, pivot joints of boom and boom cylinder on the chassis will be fixed in all directions except joint rotation direction (Figure 4.2).

4.3 Evaluation of FEA results and Convergence Check

Finite element analysis of HMK 220LC is performed under specified force and displacement boundary conditions. In this analysis, 11204 tetrahedral solid elements, 10182 quadrilateral shell elements and 37 line elements thus, total 21423 elements have been used. For shell elements, results were calculated for 5 layers through the thickness. Figure 4.7 shows the von Mises stress counter map of the boom for shell layer 1.

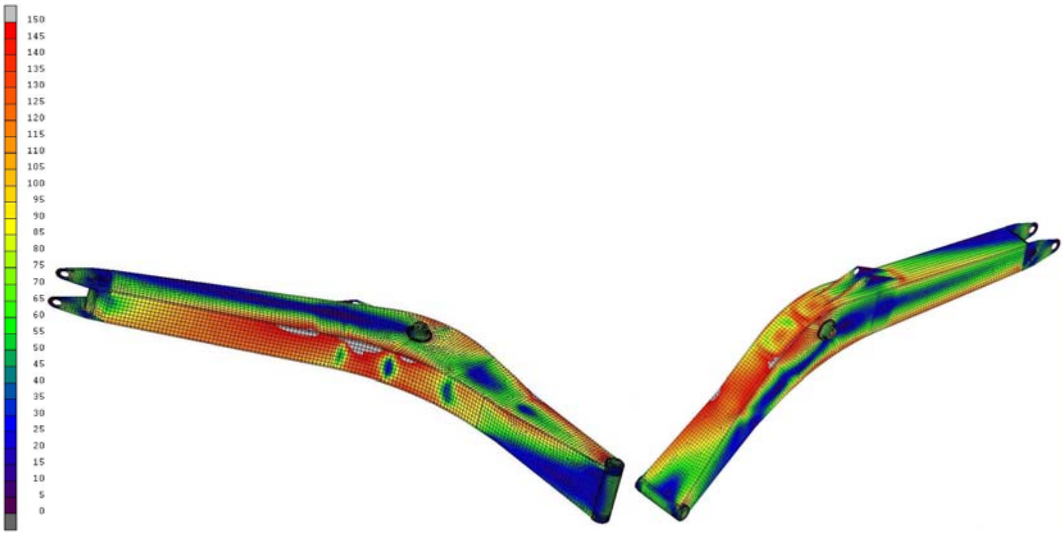

Figure 4.7: von Mises stress map for shell layer 1

In order to understand the sufficiency of total number of elements used, convergence test must be carried out. Therefore an additional analysis by using 51929 elements has been performed. Von Mises stress values of 22 critical points (Figure 4.8 and Figure 4.9) are tabulated in Table 4.1 for FEA model of the boom with 51929 and 21423 elements. Stress values at points 18, 19, 20, 21 and 22 are the von Mises stresses at shell layer 5. Other points show the von Mises stresses of the shell layer 1. As seen in Table 4.1, locations of the maximum stresses do not change when number of elements is increased. However there are differences between the stress values. Maximum percent difference between the two stress values is 7.3 % at point 21. For the preliminary design, this maximum difference was found acceptable and the analysis was carried out, using approximately 22000 elements for the excavator boom model.

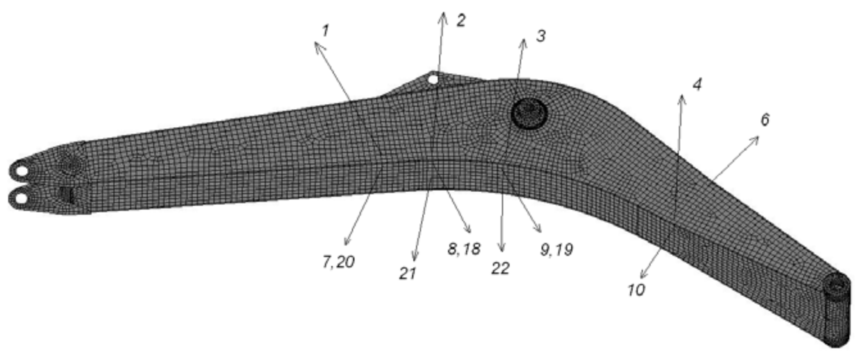

Figure 4.8: Stress points_A

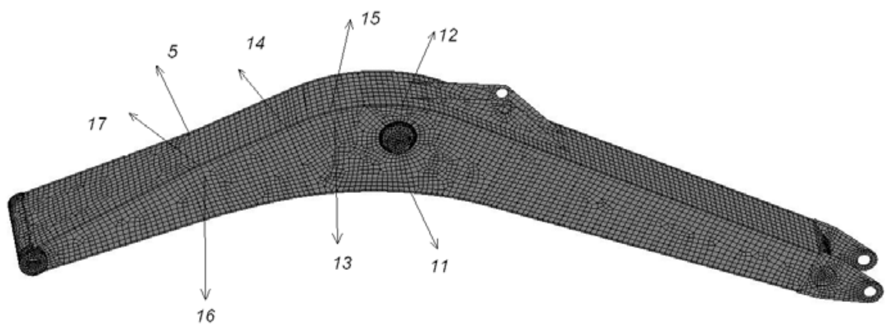

Figure 4.9: Stress points_B

Table 4.1: von Mises values of 22 points

	von Mises value (MPa)		
Point Number	Model with 21423 elements	Model with 51929 elements	Percent Difference
1	162	162	0
2	171	178	4.09
3	155	160	3.22
4	126	130	3.17
5	178	188	5.61
6	161	167	3.73
7	161	161	0
8	181	190	4.97
9	153	158	3.27
10	144	153	6.25
11	135	141	4.44
12	150	156	4.00
13	148	152	2.70
14	186	196	5.38
15	159	161	1.26
16	147	152	3.40
17	143	138	3.50
18	161	164	1.56
19	140	140	0
20	158	159	0.63
21	150	161	7.33
22	160	170	6.25
Average	155.86	160.77	3.15
Maximum	186	196	5.38

4.4 Verification of FEA by Experimental stress analysis

In order to verify the results obtained from the finite element analysis, experimental stress analysis is a useful method. At Hidromek the FE analysis results were verified by tests performed by Toprak et al. [15]. In these tests the excavator boom was placed in a specially constructed test frame. The position of the boom on this frame was the position for which the FEA was done (Figure 4.10). Using strain gauges, strains at positions that were found critical from the finite element analysis were measured from which the von Mises stress values were determined. In Figure 4.11 the von Mises stress values obtained from FE analysis and strain gauge measurements are shown. Although there are some differences between FEA and test results, correlation between the two results is satisfactory for most test points.

Figure 4.10: Test setup of the boom [15]

There are several reasons of differences between the test results and the FEA results. One of them is the measuring errors in the test. Another test based error source is the placement of the gauges to the wrong locations. Differences between the assumed material properties and their actual values can be another error source. When converting the strains (measured from the test) to von Mises stresses, modulus of elasticity is assumed as 210 GPa and the Poisson’s ratio is assumed as 0.3 for the boom material. Although these values are the accepted values for steel, modulus of elasticity and poisson's ratio may be different for the material used. Since FEA is a numerical analysis method, truncation and round-off errors will always exist as the FEA based errors. Using insufficient number of elements in the FEA modeling of the boom may be another FEA based error. Manufacturing errors causes differences between FEA model and manufactured test prototype thus result in error between measured and calculated stress values. In the test, excavator is subjected to force from the bucket by means of a hydraulic cylinder working under known maximum pressure. Errors in positioning of the cylinder and fluctuations in working pressure of this cylinder may cause differences in the boundary conditions applied in the test and the FEA.

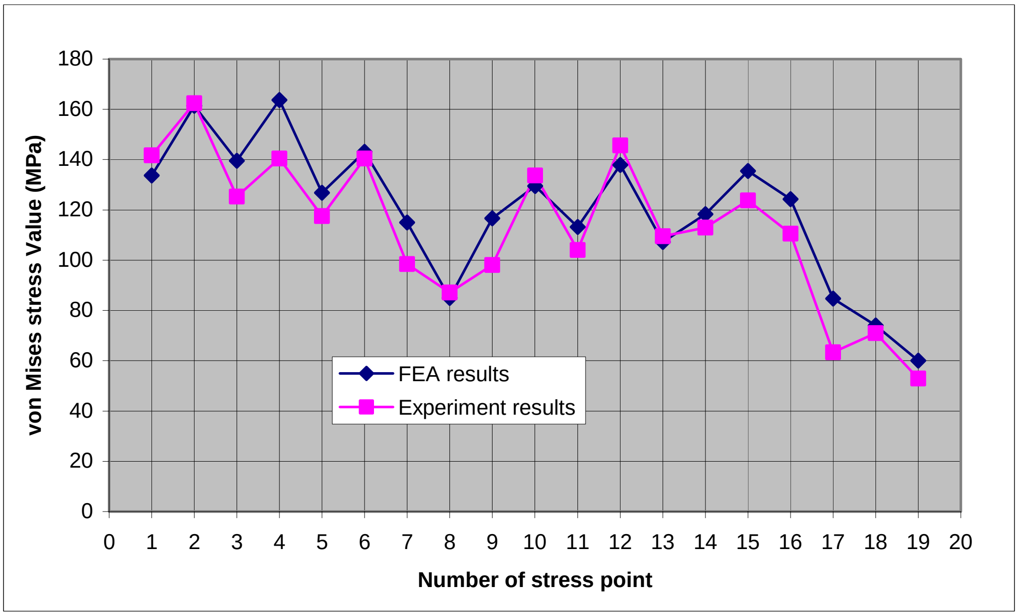

Figure 4.11: Comparison of FEA and experimental results [15]

CHAPTER 5

PARAMETRIC DESCRIPTION OF THE BOOM GEOMETRY

Finite element analysis of the HMK 220LC boom has been carried out and details of this analysis has been explained in Ch 4. By using FEA, different boom geometries can be modeled and analyzed. For the optimization of the boom for strength and cost, different boom geometries must be formed rapidly and finite element analysis of each of these geometries must be performed. However, modeling and analysis of different geometries take considerable time when standard methods are used.

In this study, a computer interface called as OPTIBOOM has been written to facilitate the optimization of the boom by reducing the geometrical modeling time in a commercial FEA program. Designed interface takes the geometric design parameters of the boom as the input and calculates all the necessary data to create FEA geometry of the boom in MSC.Marc-Mentat. After calculating the required data, the interface creates a *.proc file which includes boom creation commands and sends this file to MSC.Marc-Mentat. *.proc file is a procedure file which can be run by Mentat.

First step in designing the OPTIBOOM is the parametrization of the boom geometry.

5.1 Parametrization of the excavator boom

In creating new boom geometries, designer should have the possibility of changing boom shape very easily by changing some geometrical parameters. These parameters are called as ‘Variable parameters’. In this work, these variable parameters are divided into three groups, which are main geometry parameters, shell thicknesses, Distances of vertical reinforcements and start and end distances of middle sidewalls.

5.1.1 Main geometry parameters

Main geometry parameters are the dimensions that define the banana shaped boom geometry. There are 6 main geometry parameters and these are α_1, α_2, α_3, α_4, R_1, R_2 where α’ s are angles of the lines drawn from points P1, P2, P3 and P4 relative to the line connecting revolute joint axes. *R*’s are radii drawn between these lines (Figure 5.1).

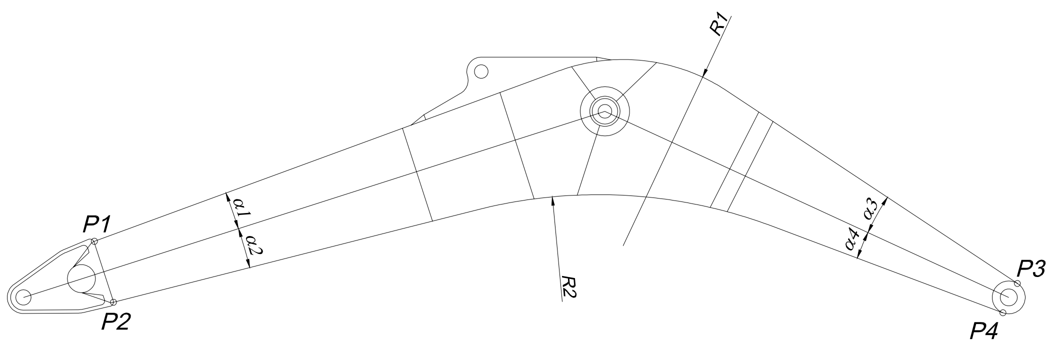

Figure 5.1: Main geometry parameters

5.1.2 Shell thicknesses

Boom is a steel structure where sheet metals of different thickness are brought together by welding. It is assumed that the boom will be constructed using 8 different panels as shown in Figure 5.2. The thicknesses of these panels are labeled as t_1, t_2, ...t_8.

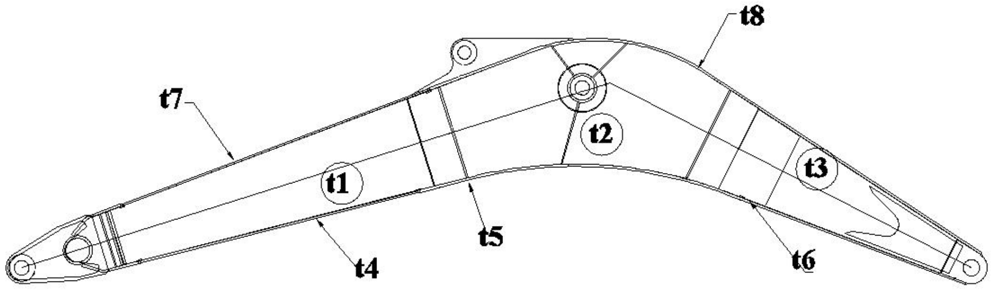

Figure 5.2: Shell thicknesses

5.1.3 Distances of vertical reinforcements and start and end distances of middle side walls

Depending on the design, there are some vertical reinforcements (Figure 5.3) in an excavator boom. According to strength and fatigue life requirements, these reinforcements can be moved inside the boom from one location to another or they can be completely removed from the assembly if the buckling of the side plates is not a critical factor.

Lengths L_1 and L_2 (Figure 5.4) are the distances of front and rear vertical reinforcements from front and rear joints of the boom. L_3 and L_4 are the distances of start and end location of middle sidewall from front and rear joints respectively.

L_{fix1} is the distance of thickness change point of upper sheet from front revolute joint of the boom. By the same way, L_{fix2} and L_{fix3} are the distances of thickness change points of the bottom sheet from back and front joints of the boom.

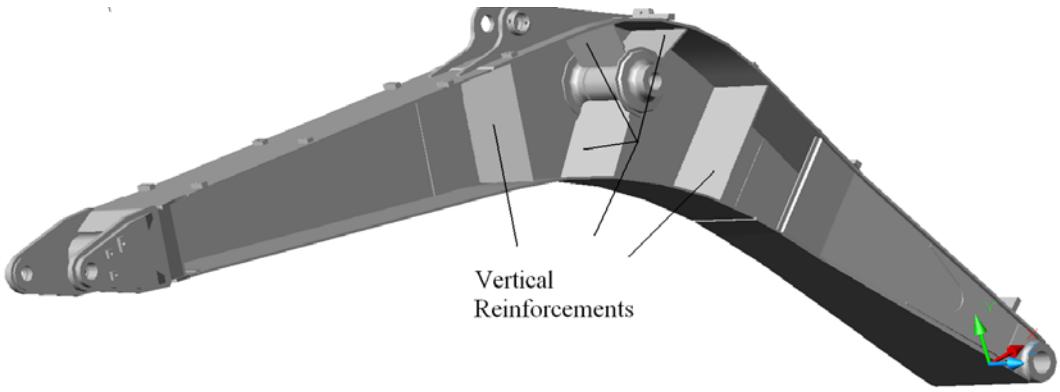

Figure 5.3: Vertical reinforcements in an excavator boom

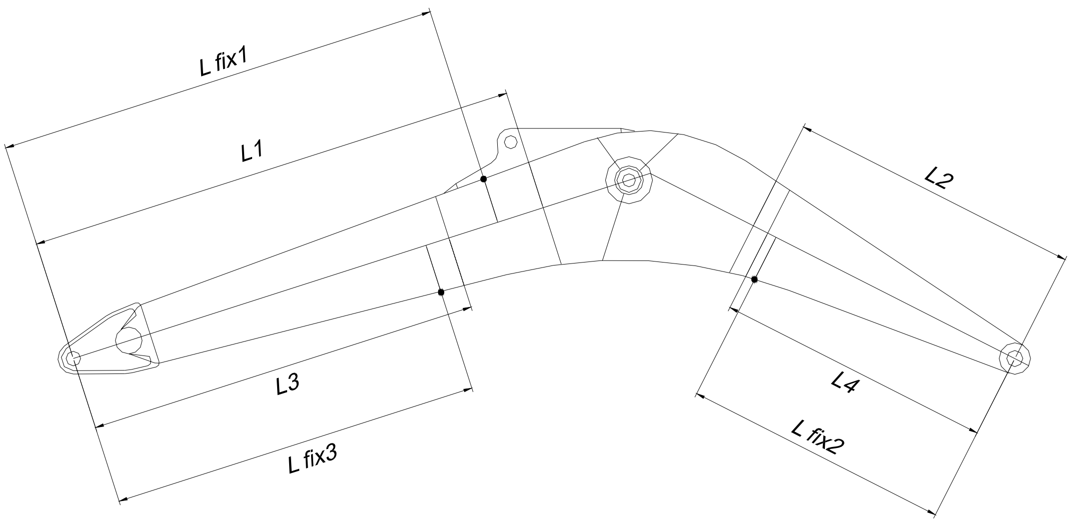

Figure 5.4: Length parameters in a boom

In designing an excavator boom, thickness, length and location of these sheets can be used as independent parameters. Designer should design new boom alternatives by changing these parameters. In this study, 21 variable design parameters are taken into account.

5.2 Fixed parts model and fixed parameters

During the design of alternative boom shapes, although boom geometry changes, excavator mechanism and joint locations do not change. Therefore, some dimensions related with the mechanism do not change throughout the design. In addition to that, it is not necessary to model the parts like boom joints, arm, bucket and connecting linkage in finite element analysis of alternative boom geometries. As a result, OPTIBOOM does not have to model these non-changing parts. An FEA model (Figure 5.5) including models of these non-changing parts can be prepared for the known excavator before OPTIBOOM is used to generate a new boom shape. This model can be superimposed with the FEA model of the boom, which will be created by the interface. The FEA model as shown in Figure 5.5 is called as ‘fixed parts model’.

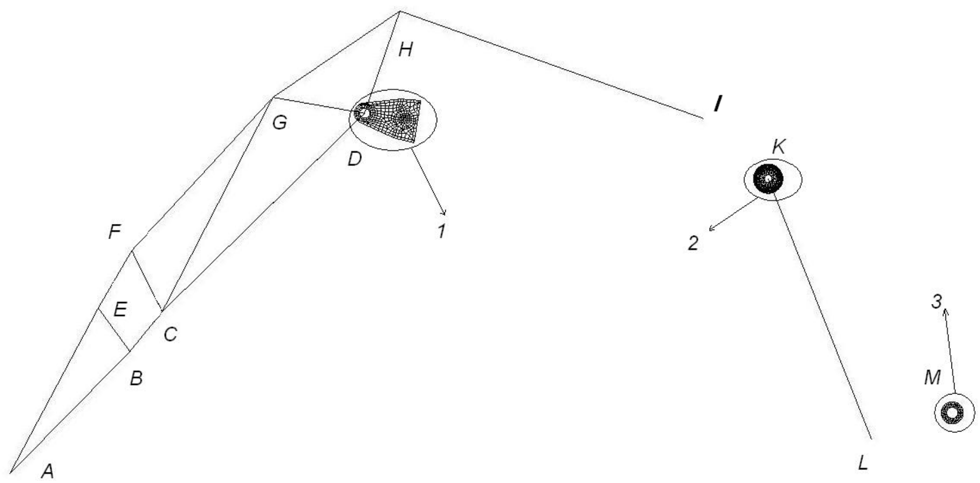

Figure 5.5: Fixed parts model of the boom

In this model, ABE is the bucket model. BE, EF FC and CB is the four bar mechanism of the excavator. B, C, G, D and H are the joint points on the arm. FG, HI and KL are the models of hydraulic cylinders. FEA models labeled as 1, 2 and 3 are the three joints of the boom, which do not change with the selected geometric parameters of the boom. Points D, K and M are the joints of the boom and L is the location where boom cylinder is attached to the frame.

Depending on the excavator mechanism and fixed parts model, there are points and dimensions (Figure 5.6 and Figure 5.7) called as *'Fixed parameters'* on the boom geometry. Coordinates of these points are known with respect to imaginary coordinate system. This coordinate system has been selected after positioning the boom according to analysis position explained in Ch 4.

α_{fix3}, α_{fix4} and α_{fix5} are the fixed angles of middle reinforcements relative to the line connecting the revolute joint axes and the orientation of these reinforcements will be kept constant throughout the analyses. L_{fix4} and L_{fix5} are the distances of intersection points of cylinder holder with the upper sheet of the boom from front joint of the boom.

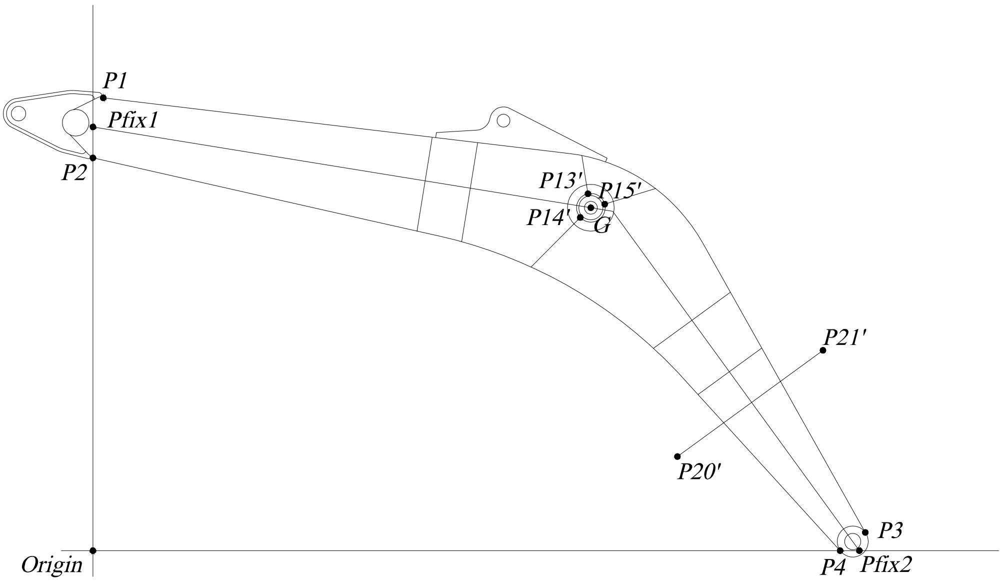

Figure 5.6: Fixeded points and origin in boom model

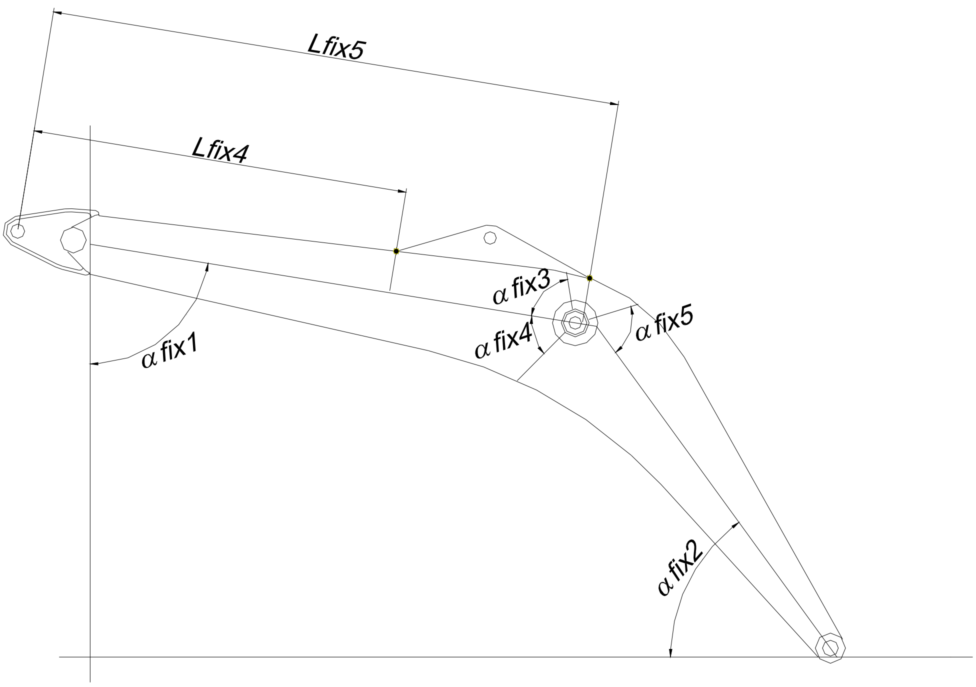

Figure 5.7: Fixed dimensions in boom model

5.3 Parametric drawing of boom geometry

Boom geometry can be defined by fixed and variable parameters. However, in order to create the FEA geometry automatically, some additional coordinates and dimensions like intersection points of lines and curves (Figure 5.8) must be calculated. In MSC.Mentat, start and end points of a line must be known to plot this line. To draw a curve, radius of the curvature must also be known in addition to start and end points of that curve. After plotting the lines and the curves in Mentat, FEA geometry can be created. Calculation of these point coordinates will be analyzed separately.

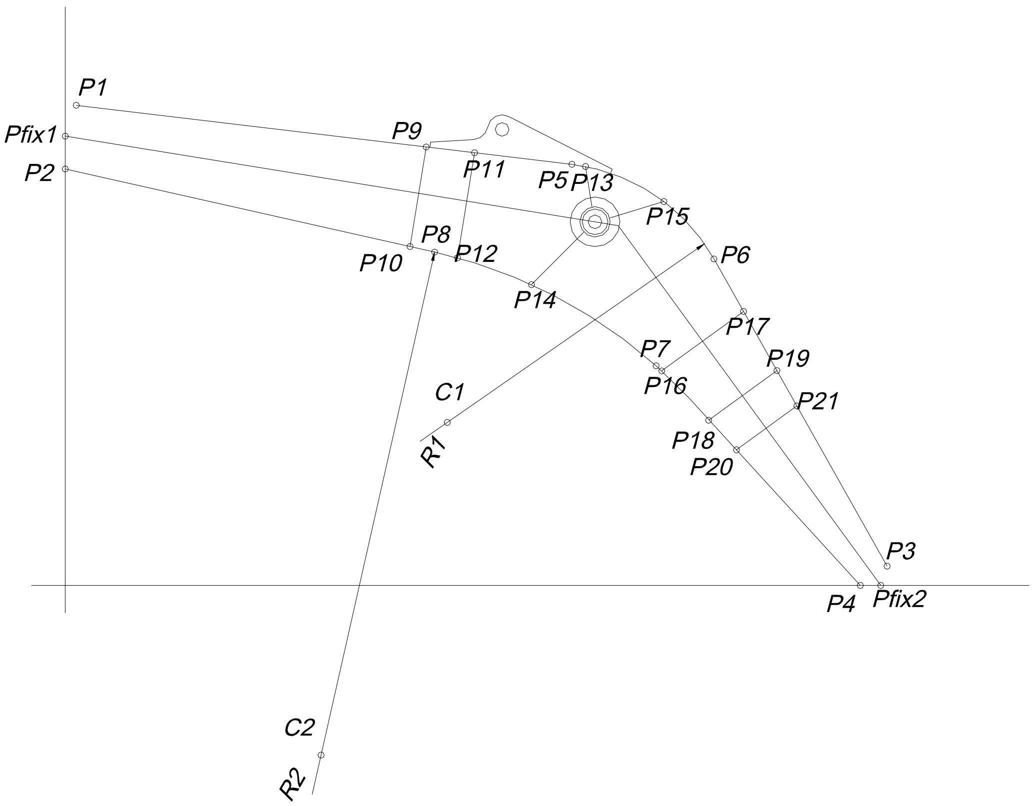

Figure 5.8: Points of intersections

5.3.1 Coordinates of points P_7, P_8, C_2, P_5, P_6 and C_1

Coordinates of points P_7, P_8 and C_2 can be found by solving loop closure equation of the loop shown in Figure 5.9, which is;

$$\overrightarrow{P_4P_7} + \overrightarrow{P_7C_2} + \overrightarrow{C_2P_8} = \overrightarrow{P_4O} + \overrightarrow{OP_2} + \overrightarrow{P_2P_8}$$

$$b_1.e^{i.(\pi-\alpha_{fix2}+\alpha_4)} + R_2.e^{i.(3\pi/2-\alpha_{fix2}+\alpha_4)} + R_2.e^{i.(\alpha_{fix1}-\alpha_2)} = -xP_4 + yP_2.i + a_1.e^{i.(3\pi/2-\alpha_{fix1}-\alpha_2)} \quad (5.1)$$

writing the real and complex parts of eq.5.1 separately 2 equations in 2 unknowns are obtained as:

$$\begin{aligned} &b_1.\cos(\pi-\alpha_{fix2}+\alpha_4) - a_1.\cos(\frac{3\pi}{2}+\alpha_{fix1}-\alpha_2) = \\ &-xP_4 - R_2.(\cos(\frac{3\pi}{2}-\alpha_{fix2}+\alpha_4)+\cos(\alpha_{fix1}-\alpha_2)) \end{aligned} \quad (5.2)$$

$$\begin{aligned} &b_1.\sin(\pi-\alpha_{fix2}+\alpha_4) - a_1.\sin(\frac{3\pi}{2}+\alpha_{fix1}-\alpha_2) = \\ &yP_2 - R_2.(\sin(\frac{3\pi}{2}-\alpha_{fix2}+\alpha_4)+\sin(\alpha_{fix1}-\alpha_2)) \end{aligned} \quad (5.3)$$

solving (5.2) and (5.3) for b_1 and a_1 gives:

$$b_1 = \frac{\begin{array}{c}(\sin(\frac{3\pi}{2}+\alpha_{fix1}-\alpha_2).(xP_4+R_2.(\cos(\frac{3\pi}{2}-\alpha_{fix2}+\alpha_4)+\cos(\alpha_{fix1}-\alpha_2)))+ \\ \cos(\frac{3\pi}{2}+\alpha_{fix1}-\alpha_2).(yP_2-R_2.(\sin(\frac{3\pi}{2}-\alpha_{fix2}+\alpha_4)+\sin(\alpha_{fix1}-\alpha_2))))\end{array}}{\sin(-\frac{\pi}{2}-\alpha_{fix1}-\alpha_{fix2}+\alpha_4+\alpha_2)}$$

$$a_1 = \frac{b_1.\cos(\pi - \alpha_{fix2} + \alpha_4) + xP_4 + R_2.(\cos(\frac{3\pi}{2} - \alpha_{fix2} + \alpha_4) + \cos(\alpha_{fix1} - \alpha_2))}{\cos(\frac{3\pi}{2} + \alpha_{fix1} - \alpha_2)} \qquad (5.4)$$

Using a_1 and b_1, coordinates of points P_7, P_8, and C_2 can be found by solving equations:

$$\begin{aligned} &yP_2.i + a_1.e^{i.(\frac{3\pi}{2}+\alpha_{fix1}-\alpha_2)} = xP_8 + i.yP_8 \\ &xP_4 + b_1, e^{i.(\pi-\alpha_{fix2}+\alpha_4)} = xP_7 + i.yP_7 \\ &xC_2 + i.yC_2 = yP_2.i + e^{i.(\frac{3\pi}{2}+\alpha_{fix1}-\alpha_2)}.a_1 + R_2.e^{i.(\pi+\alpha_{fix1}-\alpha_2)} \end{aligned} \qquad (5.5)$$

solving for the coordinates of the points;

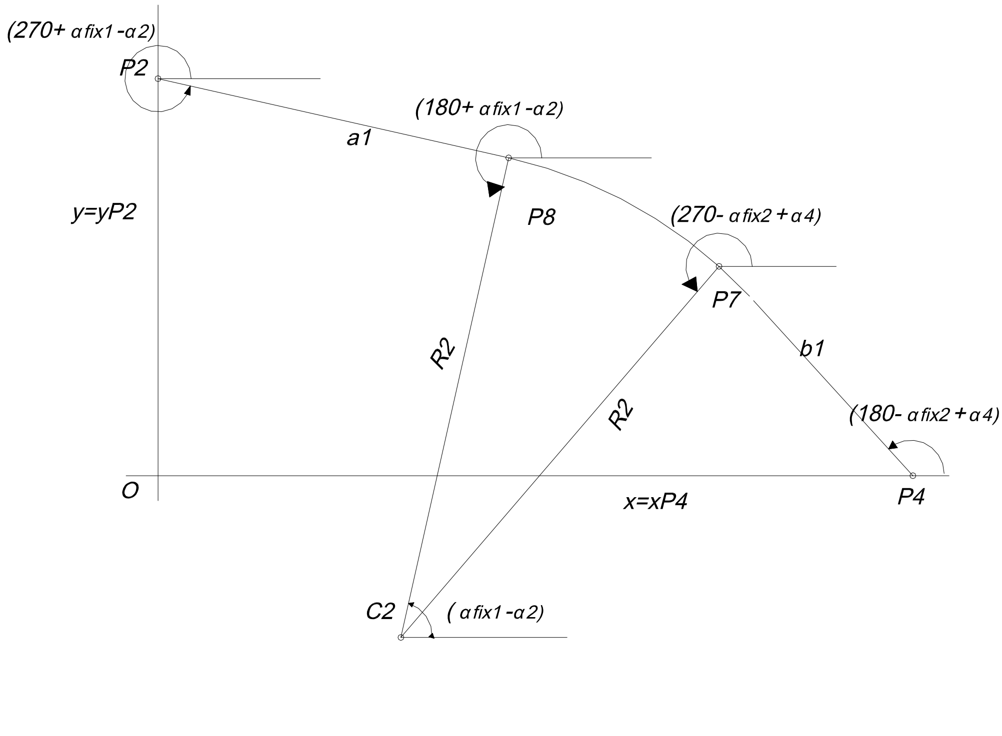

Figure 5.9: Loop_1 in boom parametrization

$$
\begin{aligned}
xP_8 &= a_1.\cos(\frac{3\pi}{2} + \alpha_{fix1} - \alpha_2) \\
yP_8 &= yP_2 + a_1.\sin(\frac{3\pi}{2} + \alpha_{fix1} - \alpha_2) \\
xP_7 &= xP_4 - b_1.\cos(\alpha_{fix2} - \alpha_4) \\
yP_7 &= b_1.\sin(\alpha_{fix2} - \alpha_4) \\
xC_2 &= a_1.\cos(\frac{3\pi}{2} + \alpha_{fix1} - \alpha_2) + R_2.\cos(\pi + \alpha_{fix1} - \alpha_2) \\
yC_2 &= yP_2 + a_1.\sin(\frac{3\pi}{2} + \alpha_{fix1} - \alpha_2) + R_2.\sin(\pi + \alpha_{fix1} - \alpha_2)
\end{aligned} \tag{5.6}
$$

To find the coordinates of points P_5, P_6, C_1, one can write the loop equation (Figure 5.10)

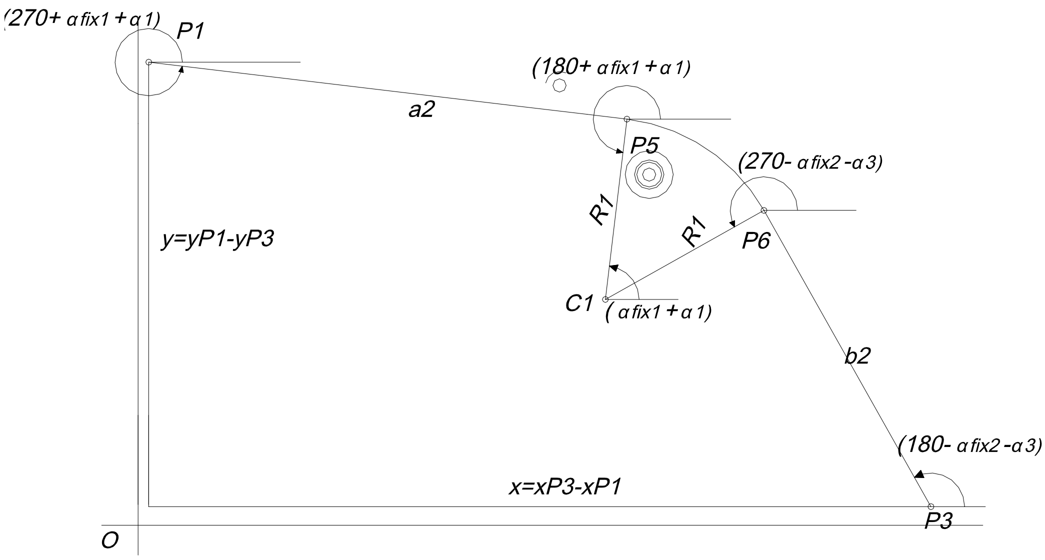

Figure 5.10: Loop_2 in boom parametrization

$$
\overrightarrow{P_3P_6} + \overrightarrow{P_6C_1} + \overrightarrow{C_1P_5} = \overrightarrow{P_3O} + \overrightarrow{OP_1} + \overrightarrow{P_1P_5}
$$

in complex numbers:

$$b_2.e^{i.(\pi-\alpha_{fix2}-\alpha_3)}+R_1.e^{i.(\frac{3\pi}{2}-\alpha_{fix2}-\alpha_3)}+R_1.e^{i.(\alpha_{fix1}+\alpha_1)}=(xP_1-xP_3)+(yP_1-yP_3)i+a_2.e^{i.(\frac{3\pi}{2}+\alpha_{fix1}+\alpha_1)} \quad (5.7)$$

applying a similar procedure to eq.(5.7) yields the coordinates of the unknown points as

$$\begin{aligned}
xP_5 &= a_2.\cos(\frac{3\pi}{2}+\alpha_{fix1}+\alpha_1)+xP_1 \\
yP_5 &= yP_1+a_2.\sin(\frac{3\pi}{2}+\alpha_{fix1}+\alpha_1) \\
xP_6 &= xP_3-b_2.\cos(\alpha_{fix2}+\alpha_3) \\
yP_6 &= b_2.\sin(\alpha_{fix2}+\alpha_3)+yP_3 \\
xC_1 &= a_2.\cos(\frac{3\pi}{2}+\alpha_{fix1}+\alpha_1)+R_1.\cos(\pi+\alpha_{fix1}+\alpha_1)+xP_1 \\
yC_1 &= yP_1+a_2.\sin(\frac{3\pi}{2}+\alpha_{fix1}+\alpha_1)+R_1.\sin(\pi+\alpha_{fix1}+\alpha_1)
\end{aligned} \quad (5.8)$$

5.3.2 Coordinates of points P_{18}, P_{19}, P_9 and P_{10}

P_{18} and P_{19} are the points where rear end point of sidewalls intersects the upper and lower shells. There are three different cases for the location of these points. First case is when $xP_7<xP_{18}$. P_7 is the ending point of bottom curvature of boom. Second case is when $xP_7>xP_{18}$ and third case is when $xP_6>xP_{19}$. P_6 is ending point of top curvature of the boom.

i) 1st case: $xP_7 < xP_{18}$ (Figure 5.11)

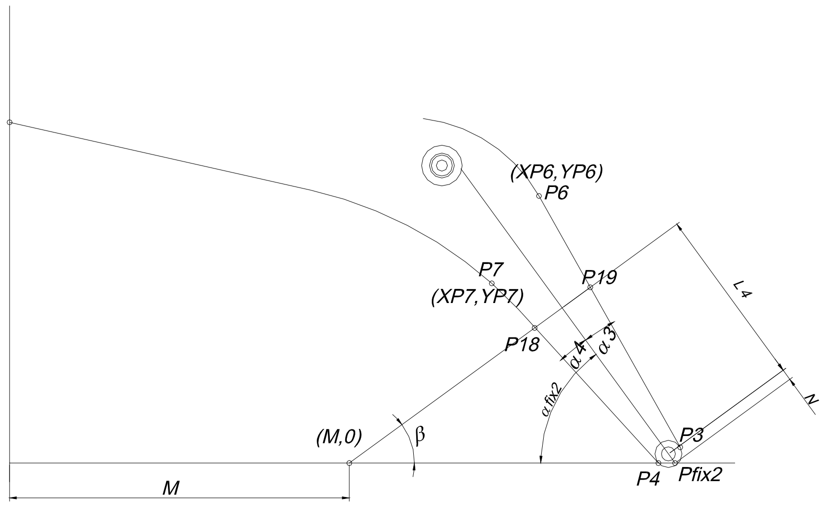

Figure 5.11: 1st case

From Figure 5.11, two equations can be written as

$$\frac{yP_{18}}{xP_4 - xP_{18}} = \tan(\alpha_{fix2} - \alpha_4) \ ;$$

$$\frac{yP_{18}}{xP_{18} - M} = \tan\beta \qquad (5.9)$$

where $\beta = \dfrac{\pi}{2} - \alpha_{fix2}$ and $M = xP_{fix2} - \dfrac{(L_4 + N_2)}{\sin\beta}$

by using equations (5.9), coordinates of P_{18} can be found as

$$xP_{18} = \frac{\tan(\alpha_{fix2} - \alpha_4).xP_4 + \tan\beta.M}{\tan\beta + \tan(\alpha_{fix2} - \alpha_4)}$$

$$yP_{18} = \tan\beta.(xP_{18} - M) \tag{5.10}$$

in Figure 5.11 $xP_6 < xP_{19}$ therefore two equations can be written to find P_{19} as

$$\frac{yP_{19} - yP_3}{xP_3 - xP_{19}} = \tan(\alpha_{fix2} + \alpha_3) \; ;$$

$$\frac{yP_{19}}{xP_{19} - M} = \tan\beta \tag{5.11}$$

solving eq.(5.11) yields

$$xP_{19} = \frac{\tan(\alpha_{fix2} + \alpha_3).xP_3 + yP_3 + \tan\beta.M}{\tan\beta + \tan(\alpha_{fix2} + \alpha_3)}$$

$$yP_{19} = \tan\beta.(xP_{19} - M) \tag{5.12}$$

ii) 2nd case: $xP_7 > xP_{18}$ (Figure 5.12)

From Figure 5.12 two equations can be written as

$$\frac{yP_{18}}{xP_{18} - M} = \tan\beta \; ;$$

$$(xP_{18} - xC_2)^2 + (yP_{18} - yC_2)^2 = R_2^2 \tag{5.13}$$

where $\beta = \frac{\pi}{2} - \alpha_{fix2}$ and $M = xP_{fix2} - \frac{(L_4 + N_2)}{\sin\beta}$

solving equation (5.13) for x and y coordinates of P_{18}:

$$xP_{18_{1,2}} = \max\left[\frac{-B \pm \sqrt{B^2 - 4.A.C}}{2A}\right]$$

$$yP_{18} = \tan\beta.(xP_{18} - M) \qquad (5.14)$$

where;

$$A = (1 + \tan^2\beta)$$
$$B = -(2.xC_2 + 2.M.\tan^2\beta + 2.yC_2.\tan\beta)$$
$$C = (xC_2{}^2 + yC_2{}^2 - R_2^2 + \tan^2\beta.M^2 + 2.yC_2.\tan\beta.M)$$

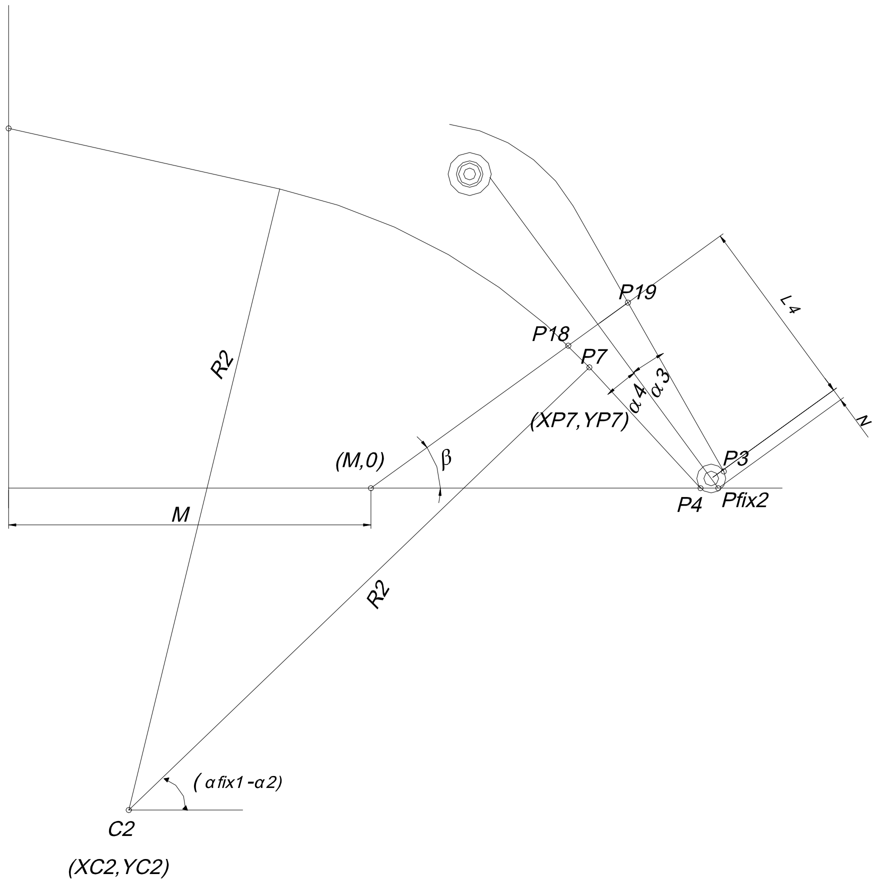

Figure 5.12: 2nd case

iii) 3rd case: $xP_6 > xP_{19}$ (Figure 5.13)

From Figure 5.13 two equations can be written as

$$\frac{yP_{19}}{xP_{19} - M} = \tan\beta \quad ;$$

$$(xP_{19} - xC_1)^2 + (yP_{19} - yC_1)^2 = R_1^{\,2} \tag{5.15}$$

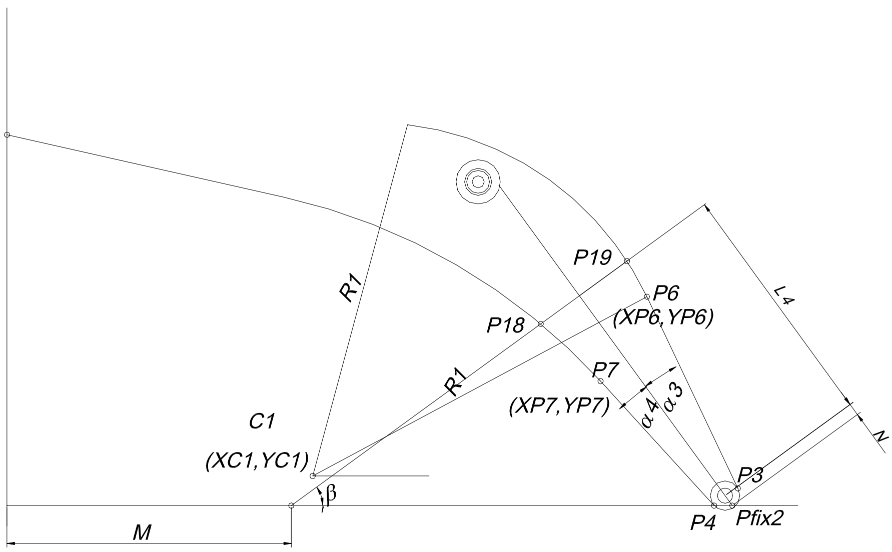

Figure 5.13: 3rd case

solving (5.15) gives

$$xP_{19_{1,2}} = \max\left[\frac{-B \pm \sqrt{B^2 - 4.A.C}}{2A}\right]$$

$$yP_{19} = \tan\beta.(xP_{19} - M) \tag{5.16}$$

where;

$$A = (1 + \tan^2 \beta)$$
$$B = -(2.xC_1 + 2.M.\tan^2 \beta + 2.yC_1.\tan \beta)$$
$$C = (xC_1^{\ 2} + yC_1^{\ 2} - R_1^2 + \tan^2 \beta.M^2 + 2.yC_1.\tan \beta.M)$$

Likewise P_{18} and P_{19}, points P_9 and P_{10} can be examined in 3 cases. P_9 and P_{10} are the points where middle sidewall starts in front of boom. The 3 cases are:

i) 1st case: $xP_{10}<xP_8$ (Figure 5.14)

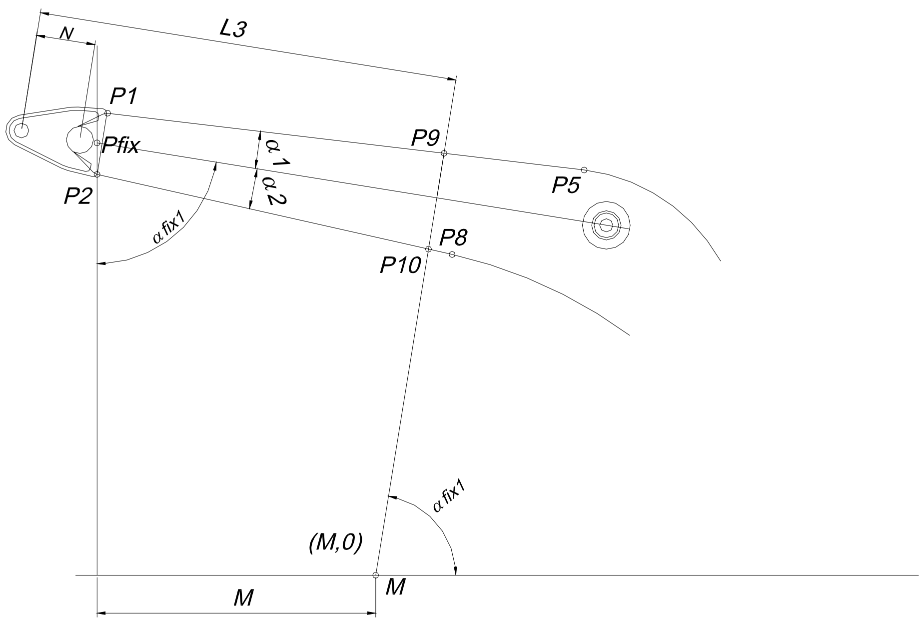

Figure 5.14: 1st case

From Figure 5.14 equations (5.17) and (5.18) can be written

$$\frac{xP_{10}}{yP_2 - yP_{10}} = \tan(\alpha_{fix1} - \alpha_2) \ ;$$

$$\frac{yP_{10}}{xP_{10} - M} = \tan\alpha_{fix1} \tag{5.17}$$

$$\frac{xP_9 - xP_1}{yP_1 - yP_9} = \tan(\alpha_{fix1} + \alpha_1) \ ;$$

$$\frac{yP_9}{xP_9 - M} = \tan\alpha_{fix1} \tag{5.18}$$

where ;

$$M = (L_3 - N_1).\sin\alpha_{fix1} - \tan(\frac{\pi}{2} - \alpha_{fix1}).(yP_{fix1} - (L_3 - N_1).\cos\alpha_{fix1})$$

from eq.(5.17) and (5.18) coordinates of points P_9 and P_{10} can be found as

$$\begin{aligned} yP_9 &= \frac{\tan\alpha_{fix1}.(yP_1.\tan(\alpha_{fix1} + \alpha_1) + xP_1) - M}{(1 + \tan\alpha_{fix1}.\tan(\alpha_{fix1} + \alpha_1))} \\ xP_9 &= \frac{yP_9}{\tan\alpha_{fix1}} + M \end{aligned} \tag{5.19}$$

$$\begin{aligned} yP_{10} &= \frac{\tan\alpha_{fix1}.(yP_2.\tan(\alpha_{fix1} - \alpha_2) - M)}{(1 + \tan\alpha_{fix1}.\tan(\alpha_{fix1} - \alpha_2))} \\ xP_{10} &= \frac{yP_{10}}{\tan\alpha_{fix1}} + M \end{aligned} \tag{5.20}$$

ii) 2^{nd} case: $xP_{10} > xP_8$ (Figure 5.15)

from Figure 5.15 two equations can be written as

$$\frac{yP_{10}}{xP_{10} - M} = \tan\alpha_{fix1} \ ;$$

$$(xP_{10} - xC_2)^2 + (yP_{10} - yC_2)^2 = R_2^{\ 2} \qquad (5.21)$$

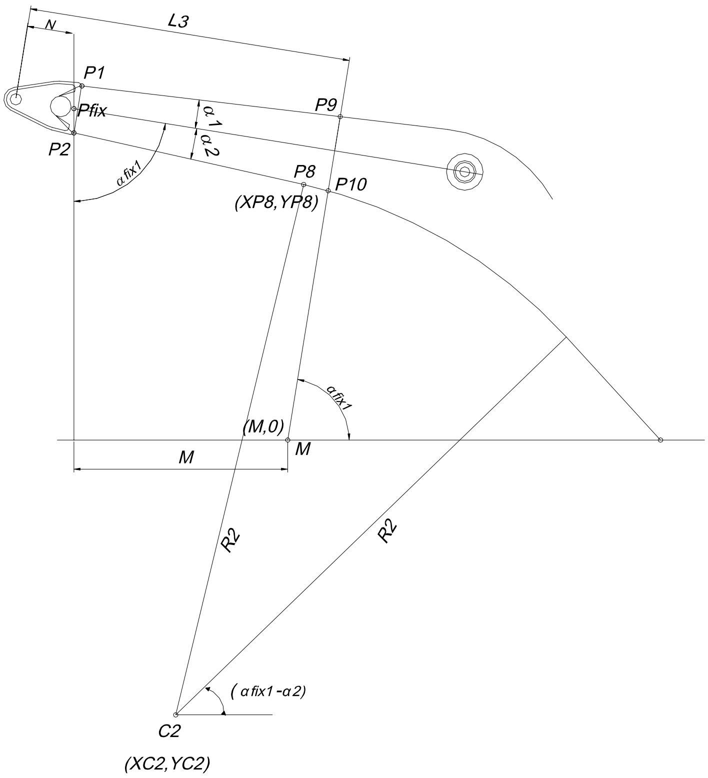

Figure 5.15: 2^{nd} case

coordinates of P_{10} can be found by solving equations in (5.21)

$$xP_{10_{1,2}} = \max\left[\frac{-B \pm \sqrt{B^2 - 4.A.C}}{2A}\right]$$

$$yP_{10} = \tan\alpha_{fix1}.(xP_{10} - M) \qquad (5.22)$$

where;

$$A = (1 + \tan^2 \alpha_{fix1})$$

$$B = -(2.xC_2 + 2.M.\tan^2 \alpha_{fix1} + 2.yC_2.\tan \alpha_{fix1})$$

$$C = (xC_2{}^2 + yC_2{}^2 - R_2^2 + \tan^2 \alpha_{fix1}.M^2 + 2.yC_2.\tan \alpha_{fix1}.M)$$

iii) 3rd case: $xP_9 > xP_5$ (Figure 5.16)

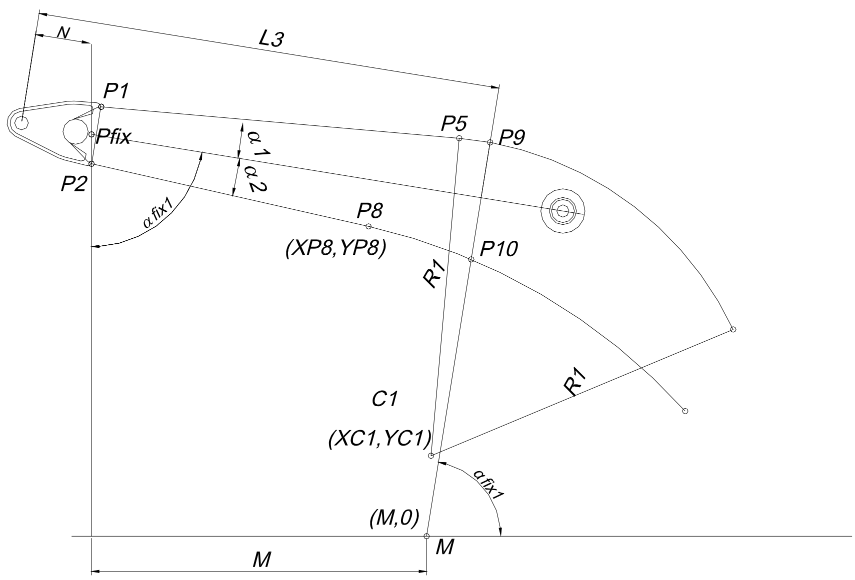

Figure 5.16: 3rd case

from Figure 5.16 two equations can be written as

$$\frac{yP_9}{xP_9 - M} = \tan \alpha_{fix1} \;;$$

$$(xP_9 - xC_1)^2 + (yP_9 - yC_1)^2 = R_1{}^2 \qquad (5.23)$$

coordinates of P_9 can be found by solving equations in (5.23)

$$xP_{9_{1,2}} = \max\left[\frac{-B \pm \sqrt{B^2 - 4.A.C}}{2A}\right]$$

$$yP_9 = \tan\alpha_{fix1}.(xP_9 - M) \tag{5.24}$$

where;

$$A = (1 + \tan^2\alpha_{fix1})$$
$$B = -(2.xC_1 + 2.M.\tan^2\alpha_{fix1} + 2.yC_1.\tan\alpha_{fix1})$$
$$C = (xC_1{}^2 + yC_1{}^2 - R_1^2 + \tan^2\alpha_{fix1}.M^2 + 2.yC_1.\tan\alpha_{fix1}.M)$$

5.3.3 Coordinates of points P_{13}, P_{14} and P_{15}

Points P_{13}, P_{14} and P_{15} are the intersection of the middle vertical reinforcements with upper and lower sheets of the boom. To determine the coordinates of these points, two different cases must be considered. In the first case, it is assumed that, reinforcement intersects the circular arcs and in the second case, it intersects the lines forming the upper and lower portion of the boom.

i) Intersection of reinforcements with circular arcs

According to Figure 5.17, 2 equations can be written for each unknown points. Therefore coordinates of points can be found from these equations.
To determine the coordinates of **P_{13}:**

$$\frac{yP_{13} - yP_{13}'}{xP_{13}' - xP_{13}} = \tan\left(\frac{\pi}{2} - \alpha_{fix1} + \alpha_{fix3}\right) \text{ ;}$$

$$(xP_{13} - xC_1)^2 + (yP_{13} - yC_1)^2 = R_1{}^2 \tag{5.25}$$

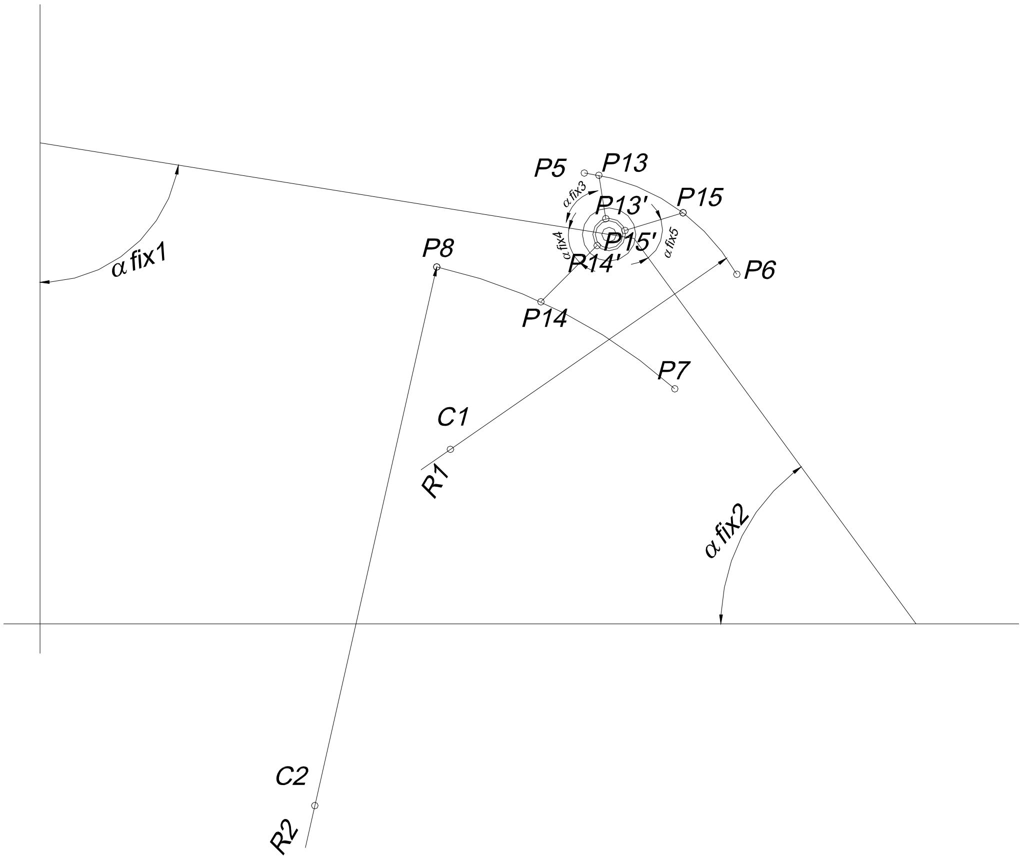

Figure 5.17: Points intersect the curvatures

solving eq.(5.25) yields:

$$xP_{13_{1,2}} = \max\left[\frac{-B \pm \sqrt{B^2 - 4.A.C}}{2A}\right]$$

$$yP_{13} = (xP_{13}^{'} - xP_{13}).\tan(\frac{\pi}{2} - \alpha_{fix1} + \alpha_{fix3}) + yP_{13}^{'} \tag{5.26}$$

where;

$$A = 1 + \tan^2(\frac{\pi}{2} - \alpha_{fix1} + \alpha_{fix3})$$

$$B = -(2.xC_1 + 2.xP_{13}^{'}.\tan^2(\frac{\pi}{2} - \alpha_{fix1} + \alpha_{fix3}) + 2.yP_{13}^{'}.\tan(\frac{\pi}{2} - \alpha_{fix1} + \alpha_{fix3})$$

$$- 2.yC_1.\tan(\frac{\pi}{2} - \alpha_{fix1} + \alpha_{fix3}))$$

$$C = (xC_1^2 + yC_1^2 - R_1^2 + (xP_{13}^{'})^2.\tan^2(\frac{\pi}{2} - \alpha_{fix1} + \alpha_{fix3})$$

$$+ 2.yP_{13}^{'}.xP_{13}^{1}.\tan(\frac{\pi}{2} - \alpha_{fix1} + \alpha_{fix3}) + yP_{13}^2 - 2.yC_1.yP_{13}^{'}$$

$$- 2.yC_1.xP_{13}^{'}.\tan(\frac{\pi}{2} - \alpha_{fix1} + \alpha_{fix3}))$$

similarly, P_{14} can be found by solving equations:

$$\frac{-yP_{14} + yP_{14}^{'}}{xP_{14}^{'} - xP_{14}} = \tan(-\frac{\pi}{2} + \alpha_{fix1} + \alpha_{fix4})\,;$$

$$(xP_{14} - xC_2)^2 + (yP_{14} - yC_2)^2 = R_2{}^2 \tag{5.27}$$

which can be solved for the coordinates as:

$$xP_{14_{1,2}} = \max\left[\frac{-B \pm \sqrt{B^2 - 4.A.C}}{2A}\right]$$

$$yP_{14} = -(xP_{14}^{'} - xP_{14}).\tan(-\frac{\pi}{2} + \alpha_{fix1} + \alpha_{fix4}) + yP_{14}^{'} \tag{5.28}$$

where;

$$A = 1 + \tan^2(\alpha_{fix1} + \alpha_{fix4} - \frac{\pi}{2})$$

$$B = -(2.xC_2 + 2.xP_{14}^{'}.\tan^2(\alpha_{fix1} + \alpha_{fix4} - \frac{\pi}{2}) + 2.yP_{14}^{'}.\tan(\alpha_{fix1} + \alpha_{fix4} - \frac{\pi}{2})$$
$$- 2.yC_2.\tan(\alpha_{fix1} + \alpha_{fix4} - \frac{\pi}{2}))$$
$$C = (xC_2^2 + yC_2^2 - R_2^2 + (xP_{14}^{'})^2.\tan^2(\alpha_{fix1} + \alpha_{fix4} - \frac{\pi}{2})$$
$$- 2.yP_{14}^{'}.xP_{14}^{'}\tan(\alpha_{fix1} + \alpha_{fix4} - \frac{\pi}{2}) + (yP_{14}^{1})^2 - 2.yC_2.yP_{14}^{'}$$
$$- 2.yC_2.xP_{14}^{'}.\tan(\alpha_{fix1} + \alpha_{fix4} - \frac{\pi}{2}))$$

by the same way, P_{15} can be found by solving equations (5.29)

$$\frac{yP_{15} - yP_{15}^{'}}{-xP_{15}^{'} + xP_{15}} = \tan(\alpha_{fix5} - \alpha_{fix2})$$
$$(xP_{15} - xC_1)^2 + (yP_{15} - yC_1)^2 = R_1^{\ 2} \qquad (5.29)$$

as:

$$xP_{15_{1,2}} = \max\left[\frac{-B \pm \sqrt{B^2 - 4.A.C}}{2A}\right]$$
$$yP_{15} = (-xP_{15}^{'} + xP_{15}).\tan(\alpha_{fix5} - \alpha_{fix2}) + yP_{15}^{'} \qquad (5.30)$$

where;

$$A = 1 + \tan^2(\alpha_{fix5} - \alpha_{fix2})$$
$$B = -(2.xC_1 + 2.xP_{15}^{'}.\tan^2(\alpha_{fix5} - \alpha_{fix2}) - 2.yP_{15}^{'}.\tan(\alpha_{fix5} - \alpha_{fix2})$$
$$+ 2.yC_1.\tan(\alpha_{fix5} - \alpha_{fix2}))$$

$$C = (xC_1^2 + yC_1^2 - R_1^2 + (xP_{15}^{'})^2.\tan^2(\alpha_{fix5} - \alpha_{fix2})$$
$$- 2.yP_{15}^{'}.xP_{15}^{'}\tan(\alpha_{fix5} - \alpha_{fix2}) + (yP_{15}^{1})^2 - 2.yC_1.yP_{15}^{'}$$
$$+ 2.yC_1.xP_{15}^{'}.\tan(\alpha_{fix5} - \alpha_{fix2}))$$

ii) Intersection of reinforcement with lines

According to the given parameters, points **P_{13}, P_{14}, P_{15}** may not intersect with the circular arcs. Instead of arcs, they may intersect the bottom and top lines. (Figure 5.18)

To determine the coordinates of **P_{13},** (5.31) must be solved**:**

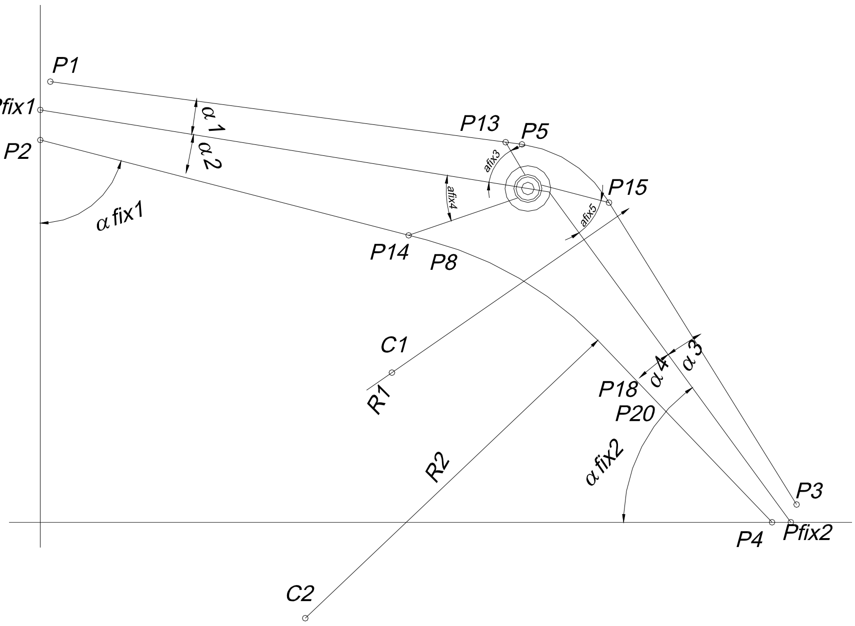

Figure 5.18: Points intersect lines

$$\frac{yP_{13} - yP_{13}^{'}}{xP_{13}^{'} - xP_{13}} = \tan\left(\frac{\pi}{2} - \alpha_{fix1} + \alpha_{fix3}\right) \; ;$$

$$\frac{xP_{13} - xP_{1}}{yP_{1} - yP_{13}} = \tan(\alpha_{fix1} + \alpha_{1}) \tag{5.31}$$

and

$$xP_{13} = \frac{xP_1 + \tan(\alpha_{fix1} + \alpha_{fix1}).(yP_1 - yP_{13}^{'} - xP_{13}^{'}.\tan(\frac{\pi}{2} - \alpha_{fix1} + \alpha_{fix3})}{1 - \tan(\frac{\pi}{2} - \alpha_{fix1} + \alpha_{fix3})} \tag{5.32}$$

$$yP_{13} = (xP_{13}^{'} - xP_{13}).\tan(\frac{\pi}{2} - \alpha_{fix1} + \alpha_{fix3}) + yP_{13}^{'}$$

To determine the coordinates of **P_{14}**, (5.33) must be solved**:**

$$\frac{yP_{14}^{'} - yP_{14}}{xP_{14}^{'} - xP_{14}} = \tan(\alpha_{fix1} + \alpha_{fix4} - \frac{\pi}{2}) \ ;$$

$$\frac{xP_{14}}{yP_2 - yP_{14}} = \tan(\alpha_{fix1} - \alpha_1) \tag{5.33}$$

and

$$xP_{14} = \frac{yP_2 + \tan(\alpha_{fix1} + \alpha_{fix4} - \frac{\pi}{2}).xP_{14}^{'} - yP_{14}^{'}}{\tan(\alpha_{fix1} + \alpha_{fix4} - \frac{\pi}{2}) + \frac{1}{\tan(\alpha_{fix1} - \alpha_{fix2})}} \tag{5.34}$$

$$yP_{13} = yP_{14}^{'} - (xP_{14}^{'} - xP_{14}).\tan(\alpha_{fix1} + \alpha_{fix4} - \frac{\pi}{2})$$

By the same way, **P_{15}** can be found by solving equations in (5.35)

$$\frac{yP_{15} - yP_{15}^{'}}{xP_{15} - xP_{15}^{'}} = \tan(\alpha_{fix5} - \alpha_{fix2}) \ ;$$

$$\frac{yP_{15} - yP_3}{xP_3 - xP_{15}} = \tan(\alpha_{fix2} + \alpha_3) \tag{5.35}$$

after some calculations P_{15} can be found as

$$xP_{15} = \frac{\tan(\alpha_{fix5} - \alpha_{fix2}).(xP_{15}^{'} + xP_3) - yP_{15}^{'} + yP_3}{\tan(\alpha_{fix5} - \alpha_{fix2}) + \tan(\alpha_{fix2} + \alpha_{fix3})}$$

$$yP_{15} = (xP_3 - xP_{15}).\tan(\alpha_{fix2} + \alpha_3) + yP_3 \tag{5.36}$$

5.3.4 Coordinates of points P_{20} and P_{21}

P_{20} and P_{21} are the points where boom's section starts to enlarge. To find the coordinates of these points, two equations can be written according to Figure 5.19

$$\frac{xP_{20} - xP_{20}^{'}}{xP_{20}^{'} - xP_{21}^{'}} = \frac{yP_{20} - yP_{20}^{'}}{yP_{20}^{'} - yP_{21}^{'}} \quad ;$$

$$\frac{yP_{20}}{xP_4 - xP_{20}} = \tan(\alpha_{fix2} - \alpha_4) \tag{5.37}$$

$$\frac{xP_{20} - xP_{20}^{'}}{xP_{20}^{'} - xP_{21}^{'}} = \frac{yP_{20} - yP_{20}^{'}}{yP_{20}^{'} - yP_{21}^{'}} \quad ;$$

$$\frac{yP_{21} - yP_3}{xP_3 - xP_{21}} = \tan(\alpha_{fix2} + \alpha_3) \tag{5.38}$$

Solving equations (5.37) and (5.38) gives the points coordinates of **P_{20} and P_{21}**

$$xP_{20} = \frac{\tan(\alpha_{fix2} - \alpha_4).(xP_{20}^{'} - xP_{21}^{'}).xP_4 + (yP_{20}^{'}.xP_{21}^{'} - xP_{20}^{'}.yP_{21}^{'})}{(yP_{20}^{'} - yP_{21}^{'}) + \tan(\alpha_{fix2} - \alpha_4).(xP_{20}^{'} - xP_{21}^{'})}$$

$$yP_{20} = \tan(\alpha_{fix2} - \alpha_4).(xP_4 - xP_{20}) \tag{5.39}$$

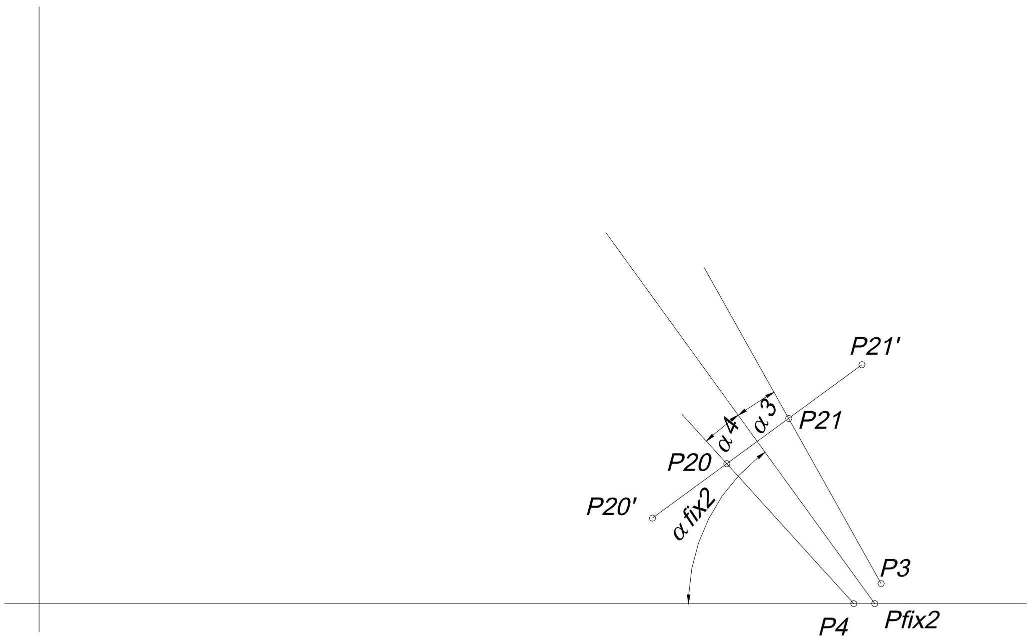

Figure 5.19: Finding points P_{20} and P_{21}

$$xP_{21} = \frac{(xP'_{20} - xP'_{21}).(\tan(\alpha_{fix2} + \alpha_3).xP_3 + yP_3) + yP'_{20}.xP'_{21} - xP'_{20}.yP'_{21}}{(yP'_{20} - yP'_{21}) + \tan(\alpha_{fix2} + \alpha_3).(xP'_{20} - xP'_{21})}$$

$$yP_{21} = \tan(\alpha_{fix2} + \alpha_3).(xP_3 - xP_{21}) + yP_3 \tag{5.40}$$

5.3.5 Coordinates of points P_{22}, P_{23}, P_{24}, P_{25} and P_{26} (Figure 5.20)

P_{22}, P_{23}, P_{24}, P_{25} and P_{26} can be defined by measuring L_{fixn} dimensions from joint locations like done before. Therefore there is no need to reformulate the same equations. L_n values in equations must be replaced with related L_{fixn} values.

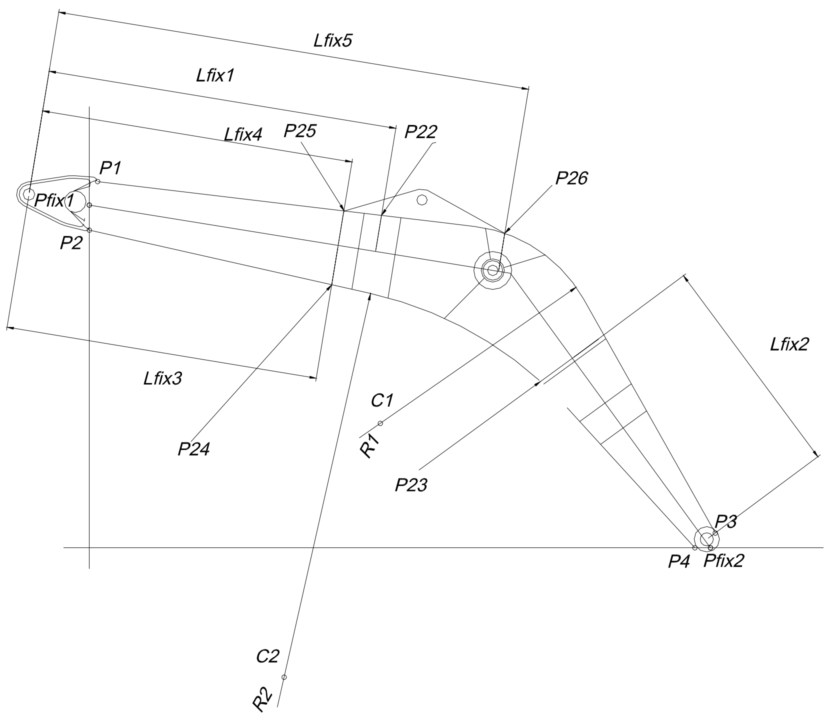

Figure 5.20: Finding points P_{22}, P_{23}, P_{24}, P_{25} and P_{26}

5.4 Working algorithm of the OPTIBOOM

Parametrization and formulation of the boom shape have been done and implemented in the OPTIBOOM (Figure 5.21). As stated at the beginning of this chapter, user must prepare a fixed parts model of the excavator mechanism, which will be used during the creation of new boom geometries. User must also define the fixed parameters of the mechanism into the interface. In the design of new boom geometry, user defines the variable parameters and the interface calculates all required data to create FEA geometry of the boom. OPTIBOOM organizes the meshing procedure of the boom by using calculated data and sends this procedure to MSC.Mentat in a *.proc file format. Mentat starts to run by opening the fixed parts model prepared by the user beforehand and creates the new boom geometry. Then, it superimposes the meshes of the boom and the fixed parts model. Flow chart of the OPTIBOOM is shown in Figure 5.23. Elements of the fixed parts model and elements of new generated boom are connected from their nodes. Figure 5.22 shows this connection. Blue meshes are the elements of fixed parts model and yellow ones are meshes of new generated boom.

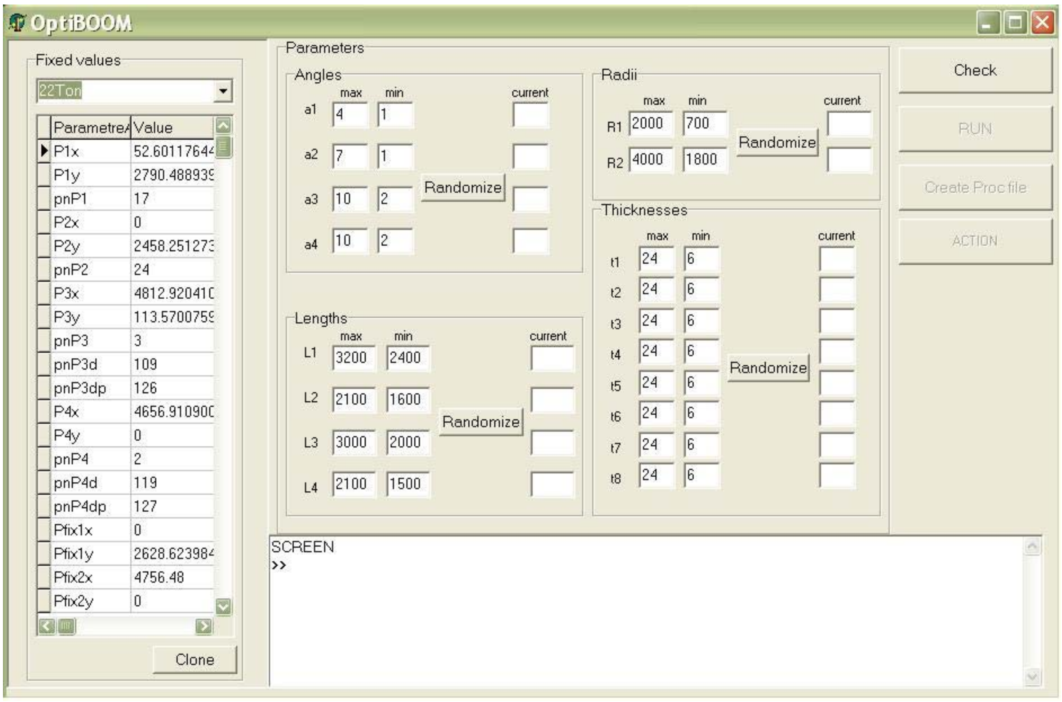

Figure 5.21: OPTIBOOM Interface

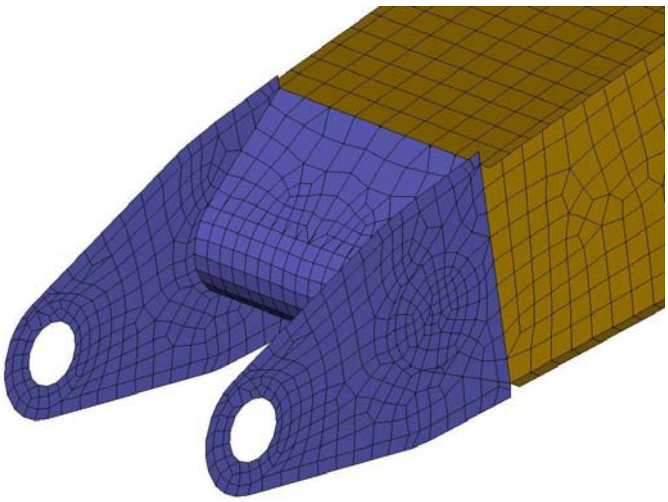

Figure 5.22: Mesh connections of fixed parts model and newly created meshes

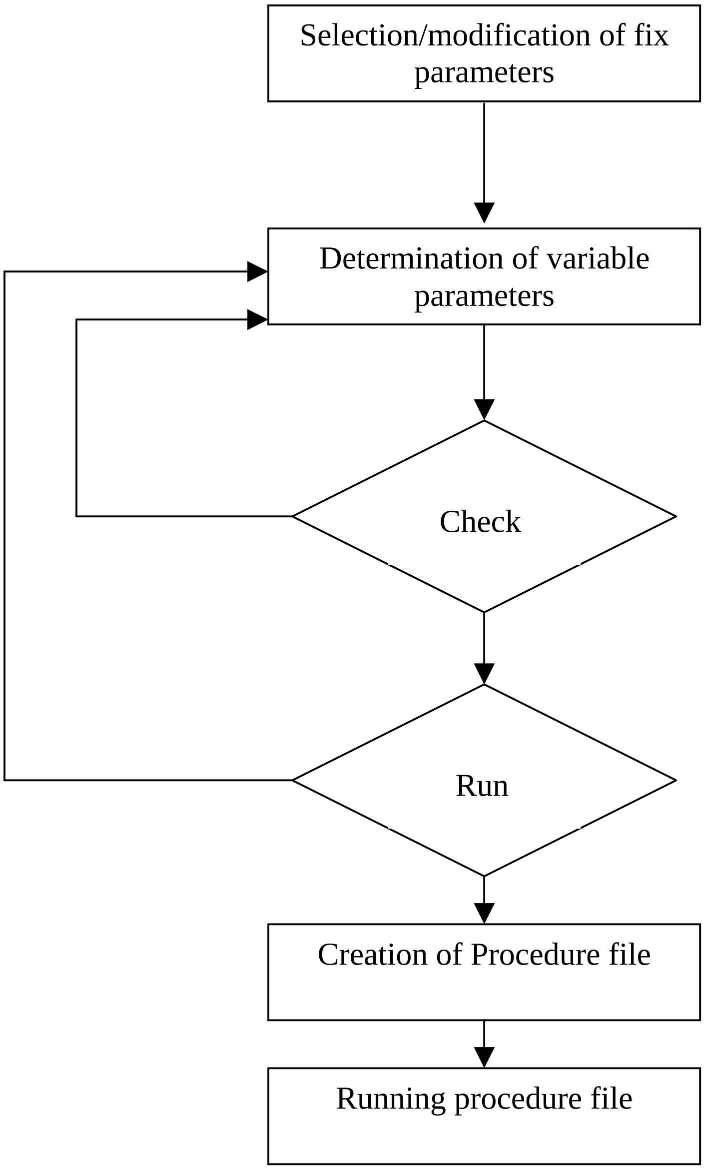

Figure 5.23: Working algorithm of the OPTIBOOM

In default fixed parts model, excavator boom is in a position where maximum breakout force is reached. Most critical stresses are expected to exist in this position. However, there may be some other critical stresses at different locations and at different positions of the mechanism. Therefore, designer must also have the possibility of changing mechanism position easily by just defining hydraulic actuator's stroke. For this reason, OPTIBOOM has been designed to change the mechanism position with little effort. User must define the cylinder strokes in fixed parameters table of the OPTIBOOM. OPTIBOOM brings the mechanism to the desired position after creating finite element model of the boom. Also, applied load for the excavator is modified since excavation force changes when the mechanism position changes.

CHAPTER 6

CASE STUDIES

OPTIBOOM has been used to improve the boom of the HMK 220 LC excavator, produced by Hidromek Ltd. Starting from an initial design, more than 100 alternative designs were created and compared with each other in terms of boom mass and maximum von Mises stresses.

The position, where excavator creates maximum breakout force by arm cylinder has been taken as the critical position for analysis. Maximum breakout force has been applied to the FEA model as boundary condition. Lateral force, which is caused by central rotation of the excavator, is also added to the force boundary condition. Determination of boundary conditions was explained in Ch 4.

Alternative boom geometries have been obtained by changing 21 variable shape parameters. In the first stage of creating alternative designs, main geometry parameters of boom have been kept same and effect of changing distances L_1 and L_2 on the stress values has been examined. After determining the effect of location of the vertical reinforcements on the stresses, main geometry parameters have been changed. Other variable parameters have also been changed to optimize the stress and mass of the boom.

As in finite element analysis of the boom explained in Ch 4, von Mises stress values of 22 different points (Figure 4.8 and Figure 4.9, pp 26) have been recorded for more than 100 alternative designs. Shape parameters and von Mises stresses of these alternatives are shown in Appendix.

To explain the design verification of HMK 220 LC excavator boom, some design alternatives and their von Mises stresses for 22 points are shown. The differences between initial design and other alternative designs are also emphasized. Initial boom shape is shown in Figure 6.1. Some selected design alternatives are models 67, 71, 74 and 90. Their shapes are also shown in Figures 6.2, 6.3, 6.4 and 6.5. The design parameters of these shapes are also tabulated in Table 6.1.

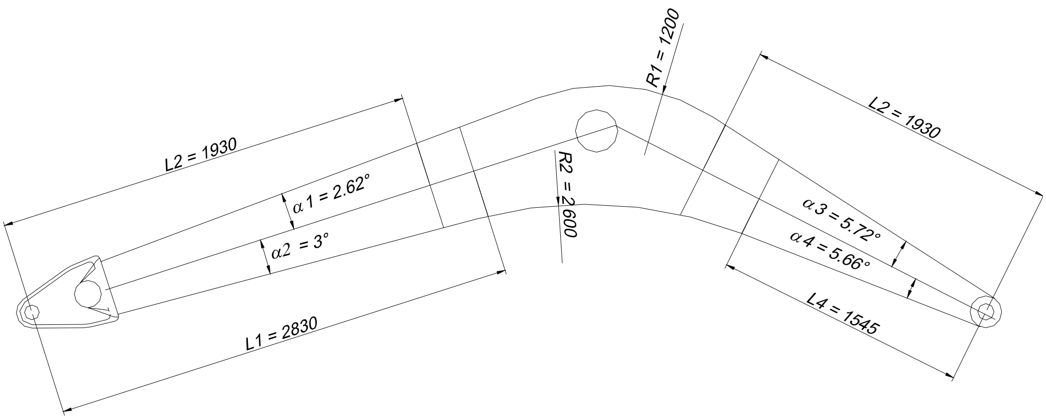

Figure 6.1: Initial design of HMK 220 LC excavator boom

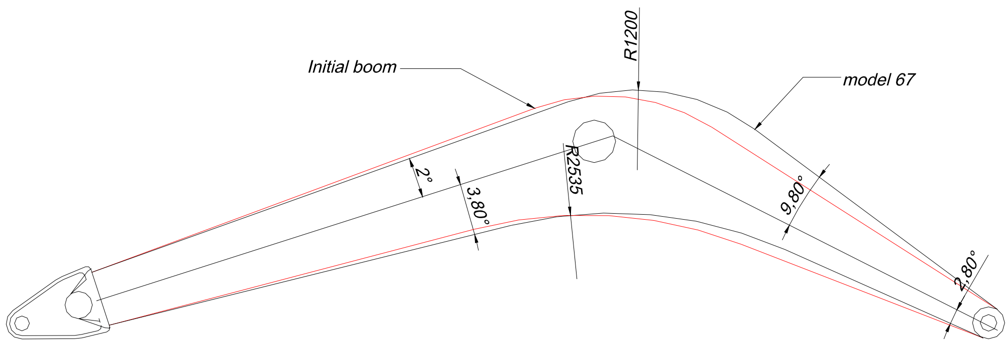

Figure 6.2: Initial boom shape and shape of model 67

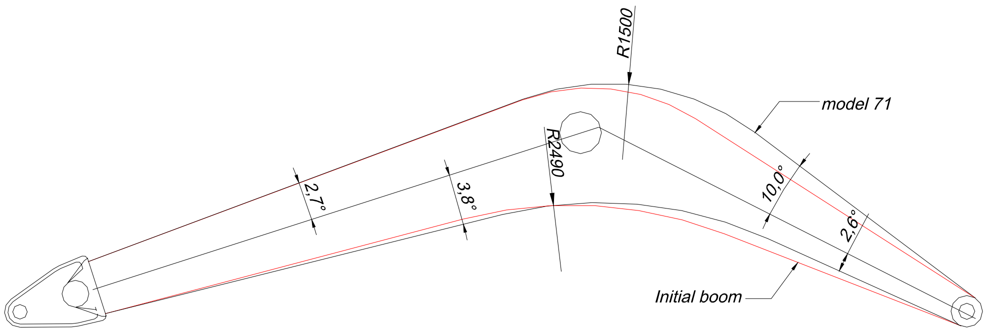

Figure 6.3: Initial boom shape and shape of model 71

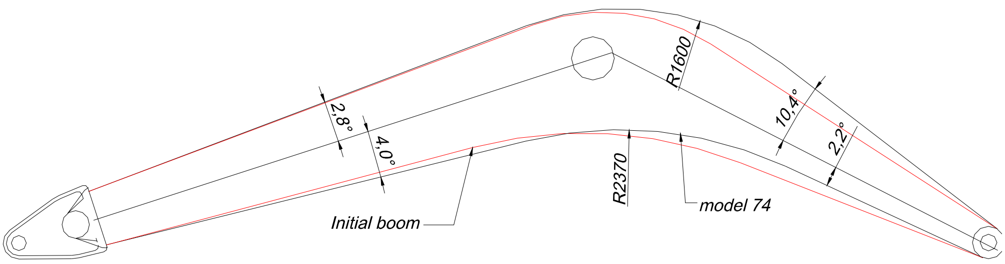

Figure 6.4: Initial boom shape and shape of model 74

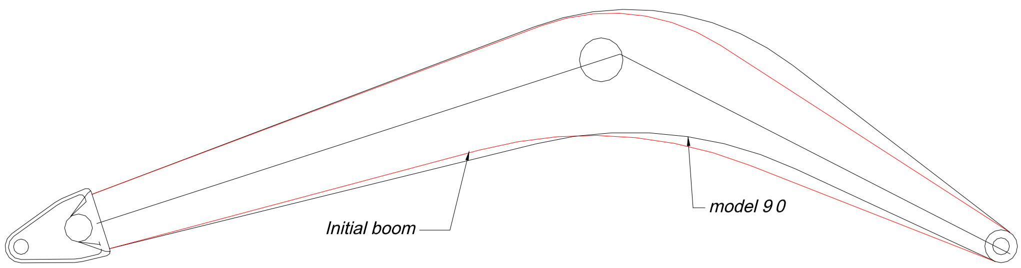

Figure 6.5: Initial boom shape and shape of model 90

Main geometry parameters of 90th model are very similar with 74th model. However changing other design parameters result in decreasing the boom mass with the same strength properties. Table 6.2 shows the stress values of 22 points for the given models.

Table 6.1: Design parameters of models

Parameters	**Design Alternatives**			
	Initial	**67**	**71**	**74**
α_1 **(Degree)**	2.62	2	2.7	2.8
α_2 **(Degree)**	3	3.8	3.8	4
α_3 **(Degree)**	5.72	9.8	10	10.4
α_4 **(Degree)**	5.66	2.8	2.6	2.2
R_1 **(mm)**	1200	1200	1500	1600
R_2 **(mm)**	2600	2535	2490	2370
L_1 **(mm)**	2830	2900	2900	2900
L_2 **(mm)**	1930	1700	1700	1700
L_3 **(mm)**	2550	2380	2380	2380
L_4 **(mm)**	1545	1600	1600	1600
t_1 **(mm)**	10	10	10	10
t_2 **(mm)**	15	15	15	15
t_3 **(mm)**	12	12	12	12
t_4 **(mm)**	12	12	12	12
t_5 **(mm)**	12	15	15	15
t_6 **(mm)**	12	12	12	12
t_7 **(mm)**	10	10	10	10
t_8 **(mm)**	15	15	15	15
L_{fix1} **(mm)**	2690	2800	2800	2800
L_{fix2} **(mm)**	1727	1800	1800	1800
L_{fix3} **(mm)**	2400	2200	2200	2200

Table 6.2: von Mises stresses at given points

Stress location	Design Alternatives				
	Initial	**67**	**71**	**74**	**90**
Mass (kg)	1403	1464	1463	1464	1454
1 (MPa)	162	145	140	138	137
2 (MPa)	171	143	139	133	131
3 (MPa)	155	144	143	146	146
4 (MPa)	126	88	86	84	84
5 (MPa)	178	142	141	140	140
6 (MPa)	161	130	130	129	129
7 (MPa)	161	145	141	138	138
8 (MPa)	181	150	146	140	140
9 (MPa)	153	138	135	136	135
10 (MPa)	144	98	97	95	95
11 (MPa)	135	115	113	116	116
12 (MPa)	150	132	135	135	134
13 (MPa)	148	120	121	121	121
14 (MPa)	186	152	148	145	145
15 (MPa)	159	134	136	136	136
16 (MPa)	147	134	133	129	129
17 (MPa)	143	126	125	122	122
18 (MPa)	161	135	131	126	126
19 (MPa)	140	126	123	125	125
20 (MPa)	158	140	136	134	133
21 (MPa)	150	123	120	111	109
22 (MPa)	160	138	136	134	130
Average	155.86	131.73	129.77	127.86	127.32
S. Deviation	14.66	15.83	15.29	15.33	15.26
Maximum	186	152	148	146	146

According to von Mises stresses and mass of the booms, best design between more than 100 alternatives is the 90th alternative. As shown in the Table 6.2, average stress values of 22 points and standard deviation of these points are the lowest among the others in this model. Its mass is also low when compared with the other models except the initial model. Maximum von Mises stress is 146 MPa in the 90th model while it is 186 MPa in the initial boom. Mass of the initial boom is 1403 Kg and mass of the 90th model is 1454 Kg. These values show that, increase in mass of 90^{th} model is 3.6 % when compared with the initial model however decrease in maximum von Mises stress is 21.5 %. von Mises stress maps for the initial and 90^{th} booms are shown in the Figures 6.6 and Figure 6.7. These figures show the stress values more than 100 MPa.

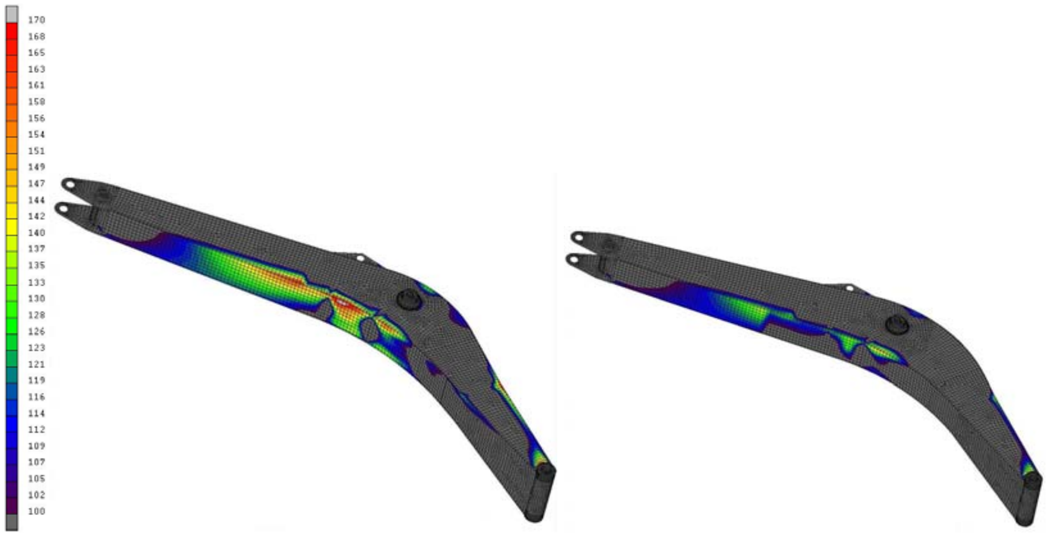

Figure 6.6: von Mises stress maps for initial (left) and 90^{th}(right) booms_A

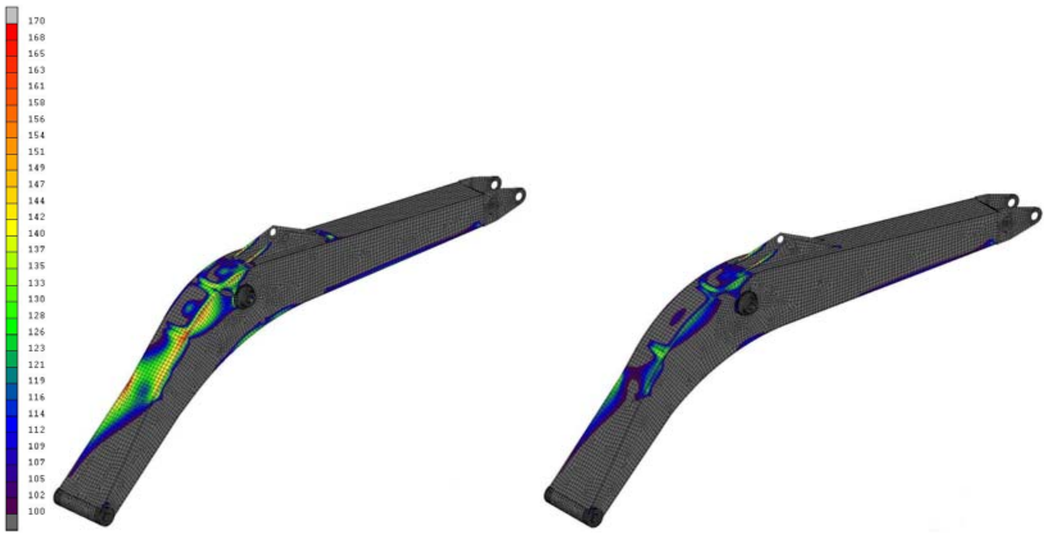

Figure 6.7: von Mises stress maps for initial (left) and 90^{th}(right) booms_B

CHAPTER 7

CONCLUSIONS

In this study, an interface, which is capable of creating finite element model of an excavator boom by using a set of design parameters, has been developed. One can then perform the finite element analysis of the boom. By using the developed software, OPTIBOOM, user can create new boom shapes and perform finite element analysis. Forces that must be applied to the boom are calculated by OPTIBOOM when mechanism position changes.

The program can be used for most of the existing boom geometries after creating a fixed parts model and defining fixed parameters related to this model.

The most important advantage of OPTIBOOM is the reduction of the modeling time. Eliminating the need for a separate CAD program and parametric definition of the boom are the main time reducing factors in the analysis. Therefore, designer can design many boom alternatives and perform FEA in a short period of time.

OPTIBOOM has been used in design modification stage of the HMK 220 LC, which is produced by Hidromek. More than 100 different design alternatives have been analyzed to minimize the maximum stresses while keeping mass of the boom around its present value. 21 shape parameters have been changed to obtain new boom geometries and the best design has been found at 90^{th} design alternative.

Maximum von Mises stress value at the 90^{th} boom is 146 MPa while it is 186 MPa in the initial boom shape. Maximum von Mises stress has been reduced by 21.5 %. Mass of the 90^{th} model is 1454 Kg and mass of the initial boom is 1403 kg. thus, mass of the boom increases only by 3.6 %.

In this study, finding the best design depends on the user, because user defines the new design parameters. Presently, optimization of the boom is not an automatic process. Therefore, implementing a logical optimization algorithm to OPTIBOOM would be a good future work. There are several optimization techniques in the literature. Some of them are explained by D. T. Pham and D. Karaboğa [14]. Genetic algorithms [21], [22], [23] locate the optima using processes similar to those in natural selection. Tabu search is a heuristic procedure [24], [25] which employs dynamically generated constraints or tabus to guide the search for optimum solutions. Another method is Neural networks [26], [27] that represent a computational models of the brain.

"Optimum" for an excavator boom is not a well defined term. Depending on the preferences, optimum may change. This will be determined when defining the objective function. The objective function may include the minimization of the maximum stress, minimization of the mass, minimization of the cost or any combination of these parameters with some weighing function.

After implementing a logical optimization algorithm to the OPTIBOOM, it would be possible to make the optimization of the boom fully automatic.

Fatigue failure of the weldments is the most important problem in the excavators. Therefore, fatigue life calculations of the weldments must also be considered. To estimate the fatigue life of the excavator boom, fracture analysis of the weldments can be carried out by sub-modeling the weld regions as in Holm's work [2]. Implementing a sub-modeling algorithm to OPTIBOOM would be another good future work.

APPENDIX

CASE STUDY TABLES

Table A.1: Design alternatives and their parameter values_1

Parameters	Design Alternatives									
	1	**2**	**3**	**4**	**5**	**6**	**7**	**8**	**9**	**10**
α_1 **(Degree)**	2.62	2.62	2.62	2.62	2.62	2.62	2.62	2.62	2.62	2.62
α_2 **(Degree)**	3	3	3	3	3	3	3	3	3	3
α_3 **(Degree)**	5.72	5.72	5.72	5.72	5.72	5.72	5.72	5.72	5.72	5.72
α_4 **(Degree)**	5.66	5.66	5.66	5.66	5.66	5.66	5.66	5.66	5.66	5.66
R_1 **(mm)**	1200	1200	1200	1200	1200	1200	1200	1200	1200	1200
R_2 **(mm)**	2600	2600	2600	2600	2600	2600	2600	2600	2600	2600
L_1 **(mm)**	2830	2650	2750	2900	3000	3100	2830	2830	2830	2900
L_2 **(mm)**	1930	1930	1930	1930	1930	1930	1700	1800	2000	1700
L_3 **(mm)**	2550	2550	2550	2550	2550	2550	2550	2550	2550	2550
L_4 **(mm)**	1545	1545	1545	1545	1545	1545	1545	1545	1545	1545
t_1 **(mm)**	10	10	10	10	10	10	10	10	10	10
t_2 **(mm)**	15	15	15	15	15	15	15	15	15	15
t_3 **(mm)**	12	12	12	12	12	12	12	12	12	12
t_4 **(mm)**	12	12	12	12	12	12	12	12	12	12
t_5 **(mm)**	12	12	12	12	12	12	12	12	12	12
t_6 **(mm)**	12	12	12	12	12	12	12	12	12	12
t_7 **(mm)**	10	10	10	10	10	10	10	10	10	10
t_8 **(mm)**	15	15	15	15	15	15	15	15	15	15
L_{fix1} **(mm)**	2690	2690	2690	2690	2690	2690	2690	2690	2690	2690
L_{fix2} **(mm)**	1727	1727	1727	1727	1727	1727	1727	1727	1727	1727
L_{fix3} **(mm)**	2400	2400	2400	2400	2400	2400	2400	2400	2400	2400

von Mises stresses at given locations for the models listed in table A.1, are shown in Table A.2. As seen from the table, changing L_1 and L_2 dimensions, results in some amount of reduction in von Mises stresses for some points but it also causes some increases in other points. Generally increasing L_1 and decreasing L_2 dimensions results in better strength characteristics. However, changing these two dimensions is not enough to reduce the stresses on the boom. Therefore, shell thickness and their start and end point dimensions should also be changed.

Table A.2: von Mises stresses at given points for design alternatives_1

Stress location	Design Alternatives									
	1	2	3	4	5	6	7	8	9	10
1 (MPa)	162	165	163	161	161	160	162	162	162	161
2 (MPa)	171	180	178	165	163	173	172	172	171	165
3 (MPa)	155	154	155	156	158	159	161	160	152	162
4 (MPa)	126	127	127	127	127	127	115	120	130	115
5 (MPa)	178	178	178	178	178	178	162	169	182	162
6 (MPa)	161	161	161	161	161	161	149	155	165	148
7 (MPa)	161	164	162	160	159	162	161	161	161	160
8 (MPa)	181	177	188	178	178	174	181	181	181	178
9 (MPa)	153	151	152	153	152	151	152	153	152	152
10 (MPa)	144	144	144	144	144	144	127	135	149	127
11 (MPa)	135	141	137	135	135	134	132	133	136	132
12 (MPa)	150	149	150	149	148	146	147	148	151	147
13 (MPa)	148	149	149	148	148	148	146	147	148	145
14 (MPa)	186	186	186	186	186	187	177	180	188	177
15 (MPa)	159	159	160	159	159	159	158	159	157	158
16 (MPa)	147	147	147	148	148	148	152	150	146	152
17 (MPa)	143	143	143	144	144	144	151	148	142	151
18 (MPa)	161	165	162	159	158	159	161	161	162	159
19 (MPa)	140	140	141	138	137	139	140	141	139	139
20 (MPa)	158	160	159	157	156	155	158	158	158	157
21 (MPa)	150	147	158	153	165	160	150	150	150	153
22 (MPa)	160	157	159	158	153	137	160	160	160	158

To see the effect of changing shell thickness and their start and end point dimensions, some alternative models have been designed. Parameters of these alternative designs are listed in Table A.3 and their FEA results are tabulated at Table A.4. Model ‘*1*’ is the initial boom design.

Table A.3: Design alternatives and their parameter values_2

Parameters	Design Alternatives						
	1	**11**	**12**	**13**	**14**	**15**	**16**
α_1 **(Degree)**	2.62	2.62	2.62	2.62	2.62	2.62	2.62
α_2 **(Degree)**	3	3	3	3	3	3	3
α_3 **(Degree)**	5.72	5.72	5.72	5.72	5.72	5.72	5.72
α_4 **(Degree)**	5.66	5.66	5.66	5.66	5.66	5.66	5.66
R_1 **(mm)**	1200	1200	1200	1200	1200	1200	1200
R_2 **(mm)**	2600	2600	2600	2600	2600	2600	2600
L_1 **(mm)**	2830	2830	2830	2830	2830	2830	2900
L_2 **(mm)**	1930	1930	1930	1930	1930	1930	1700
L_3 **(mm)**	2550	2550	2550	2550	2380	2380	2380
L_4 **(mm)**	1545	1545	1545	1545	1600	1600	1600
t_1 **(mm)**	10	10	10	10	10	10	10
t_2 **(mm)**	15	15	12	15	15	15	15
t_3 **(mm)**	12	12	12	12	12	12	12
t_4 **(mm)**	12	12	12	12	12	12	12
t_5 **(mm)**	12	15	15	15	12	15	15
t_6 **(mm)**	12	12	12	12	12	12	12
t_7 **(mm)**	10	10	10	10	10	10	10
t_8 **(mm)**	15	15	15	12	15	15	15
L_{fix1} **(mm)**	2690	2690	2690	2690	2800	2800	2800
L_{fix2} **(mm)**	1727	1727	1727	1727	1800	1800	1800
L_{fix3} **(mm)**	2400	2400	2400	2400	2200	2200	2200

Table A.4: von Mises stresses at given points for design alternatives_2

Stress location	Design Alternatives						
	1	11	12	13	14	15	16
Mass (kg)	1403	1421	1362	1382	1409	1427	1427
1 (MPa)	162	159	158	159	157	152	151
2 (MPa)	171	151	166	152	171	151	146
3 (MPa)	155	138	154	142	155	138	144
4 (MPa)	126	127	128	131	127	127	115
5 (MPa)	178	178	181	208	178	178	161
6 (MPa)	161	161	164	187	161	161	149
7 (MPa)	161	161	160	161	155	153	152
8 (MPa)	181	163	180	164	180	163	159
9 (MPa)	153	138	153	142	153	138	138
10 (MPa)	144	144	146	149	144	144	127
11 (MPa)	135	117	127	121	135	117	115
12 (MPa)	150	146	166	162	150	146	143
13 (MPa)	148	146	168	158	149	146	143
14 (MPa)	186	184	203	204	187	185	178
15 (MPa)	159	156	183	169	159	156	155
16 (MPa)	147	148	145	168	147	147	152
17 (MPa)	143	143	141	168	143	143	151
18 (MPa)	161	143	157	144	161	143	141
19 (MPa)	140	126	136	129	140	126	125
20 (MPa)	158	155	154	155	153	147	146
21 (MPa)	150	132	144	134	147	131	133
22 (MPa)	160	143	160	146	160	143	140

According to these results, it can be concluded that, increasing the thickness of t_5 from 12 mm to 15 mm, decreases the critical stresses at bottom plate. Changing L_3, L_4 and $L_{fix1, 2, 3}$ dimensions could also be useful. In model 16, L_1 and L_2 have also been changed according to the results of model 10. The strength of boom has been improved with model 16 but better results could be obtained by changing main geometry parameters. Therefore, by changing main geometry parameters and keeping others constant some alternative shapes have been designed. Table A.5 shows the alternative model parameters and Table A.6 shows FEA results of these alternatives.

Table A.5: Design alternatives and their parameter values_3

Parameters	**Design Alternatives**									
	1	**17**	**18**	**19**	**20**	**21**	**22**	**23**	**24**	**25**
α_1 **(Degree)**	2.62	2.62	3	2.64	2.4	2.99	2.62	2.62	2.7	2.7
α_2 **(Degree)**	3	3.35	3	3.72	3.5	3.49	3.7	3	3.4	3.2
α_3 **(Degree)**	5.72	5.72	6.35	6.39	6.7	6.39	6.7	6.5	6.6	6.2
α_4 **(Degree)**	5.66	6.32	5.66	6.25	6.3	6.25	6	6.5	6	6
R_1 **(mm)**	1200	1200	1000	1200	1100	1150	1100	1100	1100	1100
R_2 **(mm)**	2600	2900	2600	2700	2900	2800	2950	2800	2900	3000
L_1 **(mm)**	2830	2830	2830	2830	2830	2830	2830	2830	2830	2830
L_2 **(mm)**	1930	1930	1930	1930	1930	1930	1930	1930	1930	1930
L_3 **(mm)**	2550	2550	2550	2550	2550	2550	2550	2550	2550	2550
L_4 **(mm)**	1545	1545	1545	1545	1545	1545	1545	1545	1545	1545
t_1 **(mm)**	10	10	10	10	10	10	10	10	10	10
t_2 **(mm)**	15	15	15	15	15	15	15	15	15	15
t_3 **(mm)**	12	12	12	12	12	12	12	12	12	12
t_4 **(mm)**	12	12	12	12	12	12	12	12	12	12
t_5 **(mm)**	12	12	12	12	12	12	12	12	12	12
t_6 **(mm)**	12	12	12	12	12	12	12	12	12	12
t_7 **(mm)**	10	10	10	10	10	10	10	10	10	10
t_8 **(mm)**	15	15	15	15	15	15	15	15	15	15
L_{fix1} **(mm)**	2690	2690	2690	2690	2690	2690	2690	2690	2690	2690
L_{fix2} **(mm)**	1727	1727	1727	1727	1727	1727	1727	1727	1727	1727
L_{fix3} **(mm)**	2400	2400	2400	2400	2400	2400	2400	2400	2400	2400

Table A.6: von Mises stresses at given points for design alternatives_3

Stress location	**Design Alternatives**									
	1	**17**	**18**	**19**	**20**	**21**	**22**	**23**	**24**	**25**
Mass(kg)	1403	1421	1426	1435	1439	1439	1440	1432	1437	1429
1 (MPa)	162	159	159	152	158	153	153	165	157	162
2 (MPa)	171	157	167	158	156	155	152	162	156	156
3 (MPa)	155	143	146	143	139	139	136	142	138	138
4 (MPa)	126	123	120	117	114	117	115	116	116	120
5 (MPa)	178	175	172	170	167	170	169	167	170	173
6 (MPa)	161	159	156	154	152	155	154	152	154	157
7 (MPa)	161	157	158	151	156	152	152	162	155	159
8 (MPa)	181	172	167	169	172	169	167	177	170	173
9 (MPa)	153	143	144	142	140	138	137	142	139	139
10 (MPa)	144	141	137	134	130	134	133	131	132	138
11 (MPa)	135	125	126	125	121	120	118	123	120	120
12 (MPa)	150	142	143	140	137	140	136	140	138	140
13 (MPa)	148	142	136	137	132	134	132	134	133	136
14 (MPa)	186	179	171	174	166	169	168	168	168	171
15 (MPa)	159	151	138	146	140	141	139	142	140	143
16 (MPa)	147	146	143	143	141	143	142	141	142	144
17 (MPa)	143	142	138	136	134	137	135	135	136	138
18 (MPa)	161	154	156	151	154	151	150	158	153	154
19 (MPa)	140	130	133	130	128	127	126	130	128	127
20 (MPa)	158	154	155	149	154	150	149	159	153	157
21 (MPa)	150	152	146	135	151	142	141	156	145	157
22 (MPa)	160	148	152	147	145	143	142	151	144	145

Table A.6 shows that, models 19, 20 and 22 stronger than others. However, improving strength characteristics of the boom resulted in some amount of increase of boom mass. Effects of all parameters have been examined and result of all these works can be combined. Except main geometry parameters, other parameters of models 19, 20 and 22 can be changed to obtain stronger and lighter booms. For this purpose, some alternative booms have been designed and listed in Tables. von Mises stresses of these alternatives have been also tabulated in the Tables.

Table A.7: Parameters of model 19 and its derivatives

Parameters	Design Alternatives									
	19	**26**	**27**	**28**	**29**	**30**	**31**	**32**	**33**	**34**
α_1 **(Degree)**	2.64	2.64	2.64	2.64	2.64	2.64	2.64	2.64	2.64	2.64
α_2 **(Degree)**	3.72	3.72	3.72	3.72	3.72	3.72	3.72	3.72	3.72	3.72
α_3 **(Degree)**	6.39	6.39	6.39	6.39	6.39	6.39	6.39	6.39	6.39	6.39
α_4 **(Degree)**	6.25	6.25	6.25	6.25	6.25	6.25	6.25	6.25	6.25	6.25
R_1 **(mm)**	1200	1200	1200	1200	1200	1200	1200	1200	1200	1200
R_2 **(mm)**	2700	2700	2700	2700	2700	2700	2700	2700	2700	2700
L_1 **(mm)**	2830	2830	2830	3000	3000	3000	3000	2900	3000	2900
L_2 **(mm)**	1930	1930	1930	1800	2000	1800	2000	1700	1800	1850
L_3 **(mm)**	2550	2550	2550	2550	2550	2550	2550	2380	2380	2380
L_4 **(mm)**	1545	1545	1545	1545	1545	1545	1545	1600	1600	1600
t_1 **(mm)**	10	10	10	10	10	10	10	10	10	10
t_2 **(mm)**	15	15	12	12	12	15	15	15	15	15
t_3 **(mm)**	12	12	12	12	12	12	12	12	12	12
t_4 **(mm)**	12	12	12	12	12	12	12	12	12	12
t_5 **(mm)**	12	15	15	15	15	15	15	15	15	15
t_6 **(mm)**	12	12	12	12	12	12	12	12	12	12
t_7 **(mm)**	10	10	10	10	10	10	10	10	10	10
t_8 **(mm)**	15	15	15	15	15	15	15	15	15	15
L_{fix1} **(mm)**	2690	2690	2690	2690	2690	2690	2690	2800	2800	2800
L_{fix2} **(mm)**	1727	1727	1727	1727	1727	1727	1727	1800	1800	1800
L_{fix3} **(mm)**	2400	2400	2400	2400	2400	2400	2400	2200	2200	2200

Table A.8: von Mises stresses of model 19 and its derivatives

Stress location	Design Alternatives									
	19	**26**	**27**	**28**	**29**	**30**	**31**	**32**	**33**	**34**
Mass(kg)	1435	1452	1389	1389	1389	1452	1452	1455	1455	1455
1 (MPa)	152	150	148	146	146	147	145	142	141	142
2 (MPa)	158	141	155	148	149	136	136	137	136	137
3 (MPa)	143	128	143	150	142	134	127	134	134	131
4 (MPa)	117	117	117	112	122	111	121	106	111	113
5 (MPa)	170	170	172	163	177	161	174	154	167	164
6 (MPa)	154	155	157	150	160	148	158	142	148	150
7 (MPa)	151	151	150	148	147	148	148	143	141	143
8 (MPa)	169	152	168	166	166	150	151	151	150	151
9 (MPa)	142	128	142	142	141	130	127	129	129	129
10 (MPa)	134	133	136	126	140	124	138	117	124	128
11 (MPa)	125	108	117	116	116	106	108	105	106	107
12 (MPa)	140	137	156	153	157	134	138	133	133	135
13 (MPa)	137	131	155	154	152	133	132	131	133	134
14 (MPa)	174	172	191	181	185	166	166	166	161	169
15 (MPa)	146	143	168	170	163	143	140	142	141	144
16 (MPa)	143	139	140	143	139	145	141	146	143	142
17 (MPa)	136	136	134	139	132	141	134	144	144	139
18 (MPa)	151	134	148	144	144	132	132	133	132	133
19 (MPa)	130	118	128	129	126	116	116	117	117	116
20 (MPa)	149	146	145	142	142	143	143	138	136	138
21 (MPa)	135	119	135	145	145	132	132	123	131	123
22 (MPa)	147	131	147	136	135	123	122	131	123	131

Table A.9: Parameters of model 20 and its derivatives

Parameters	Design Alternatives									
	20	**35**	**36**	**37**	**38**	**39**	**40**	**41**	**42**	**43**
α_1 **(Degree)**	2.4	2.4	2.4	2.4	2.4	2.4	2.4	2.4	2.4	2.4
α_2 **(Degree)**	3.5	3.5	3.5	3.5	3.5	3.5	3.5	3.5	3.5	3.5
α_3 **(Degree)**	6.7	6.7	6.7	6.7	6.7	6.7	6.7	6.7	6.7	6.7
α_4 **(Degree)**	6.3	6.3	6.3	6.3	6.3	6.3	6.3	6.3	6.3	6.3
R_1 **(mm)**	1100	1100	1100	1100	1100	1100	1100	1100	1100	1100
R_2 **(mm)**	2900	2900	2900	2900	2900	2900	2900	2900	2900	2900
L_1 **(mm)**	2830	2830	2830	2900	2900	2762	2980	2700	2720	2950
L_2 **(mm)**	1930	1930	1930	1700	1700	1803	1780	1800	1780	1800
L_3 **(mm)**	2550	2550	2550	2380	2380	2555	2720	2550	2160	2350
L_4 **(mm)**	1545	1545	1545	1600	1600	1595	1720	1600	1760	1550
t_1 **(mm)**	10	10	10	10	10	10	10	10	10	10
t_2 **(mm)**	15	15	12	12	15	15	15	15	15	15
t_3 **(mm)**	12	12	12	12	12	12	12	12	12	12
t_4 **(mm)**	12	12	12	12	12	12	12	12	12	12
t_5 **(mm)**	12	15	15	15	15	15	15	15	12	15
t_6 **(mm)**	12	12	12	12	12	12	12	12	12	12
t_7 **(mm)**	10	10	10	10	10	10	10	10	10	10
t_8 **(mm)**	15	15	15	15	15	15	15	15	15	15
L_{fix1} **(mm)**	2690	2690	2690	2800	2800	2685	2800	2900	2690	2900
L_{fix2} **(mm)**	1727	1727	1727	1800	1800	1444	1800	1750	1727	1750
L_{fix3} **(mm)**	2400	2400	2400	2200	2200	2450	2200	2250	2400	2200

Table A.10: von Mises stresses of model 20 and its derivatives

Stress location	Design Alternatives									
	20	**35**	**36**	**37**	**38**	**39**	**40**	**41**	**42**	**43**
Mass(kg)	1439	1456	1393	1394	1460	1455	1442	1451	1448	1462
1 (MPa)	158	154	153	145	146	156	154	151	146	146
2 (MPa)	156	140	154	150	136	143	138	147	164	137
3 (MPa)	139	124	139	145	130	127	130	127	142	129
4 (MPa)	114	114	115	104	102	108	106	107	106	107
5 (MPa)	167	167	170	153	151	159	157	159	158	159
6 (MPa)	152	152	155	142	140	146	145	146	145	146
7 (MPa)	156	156	155	146	147	158	146	153	143	146
8 (MPa)	172	155	171	169	152	156	153	158	173	152
9 (MPa)	140	126	140	140	127	127	127	126	139	127
10 (MPa)	130	130	132	115	113	121	119	121	119	121
11 (MPa)	121	105	114	112	102	104	103	107	124	103
12 (MPa)	137	134	153	148	129	132	131	131	135	131
13 (MPa)	132	130	151	148	127	129	129	129	131	129
14 (MPa)	166	164	182	174	161	160	166	162	172	162
15 (MPa)	140	138	163	163	136	138	138	138	142	138
16 (MPa)	141	141	138	141	144	141	141	141	143	143
17 (MPa)	134	134	132	140	142	138	139	138	138	138
18 (MPa)	154	136	147	146	134	137	134	138	154	133
19 (MPa)	128	116	129	127	115	117	115	117	129	114
20 (MPa)	154	150	149	141	142	153	141	147	141	141
21 (MPa)	151	131	142	145	132	124	141	126	137	136
22 (MPa)	145	129	145	144	129	131	124	133	146	124

Table A.11: Parameters of model 22 and its derivatives

Parameters	Design Alternatives									
	22	**44**	**45**	**46**	**47**	**48**	**49**	**50**	**51**	**52**
α_1 **(Degree)**	2.62	2.62	2.62	2.62	2.62	2.62	2.62	2.62	2.62	2.62
α_2 **(Degree)**	3.7	3.7	3.7	3.7	3.7	3.7	3.7	3.7	3.7	3.7
α_3 **(Degree)**	6.7	6.7	6.7	6.7	6.7	6.7	6.7	6.7	6.7	6.7
α_4 **(Degree)**	6	6	6	6	6	6	6	6	6	6
R_1 **(mm)**	1100	1100	1100	1100	1100	1100	1100	1100	1100	1100
R_2 **(mm)**	2950	2950	2950	2950	2950	2950	2950	2950	2950	2950
L_1 **(mm)**	2830	2830	2830	2900	2900	2762	3000	2700	2560	2920
L_2 **(mm)**	1930	1930	1930	1700	1700	1803	1800	1800	2020	1755
L_3 **(mm)**	2550	2550	2550	2380	2380	2555	2450	2550	2320	2380
L_4 **(mm)**	1545	1545	1545	1600	1600	1595	1550	1600	1500	1550
t_1 **(mm)**	10	10	10	10	10	10	10	10	10	10
t_2 **(mm)**	15	15	12	12	15	15	15	15	15	15
t_3 **(mm)**	12	12	12	12	12	12	12	12	12	12
t_4 **(mm)**	12	12	12	12	12	12	12	12	12	12
t_5 **(mm)**	12	15	15	15	15	15	15	15	15	15
t_6 **(mm)**	12	12	12	12	12	12	12	12	12	12
t_7 **(mm)**	10	10	10	10	10	10	10	10	10	10
t_8 **(mm)**	15	15	15	15	15	15	15	15	15	15
L_{fix1} **(mm)**	2690	2690	2690	2800	2800	2685	2900	2900	2700	3050
L_{fix2} **(mm)**	1727	1727	1727	1800	1800	1444	1650	1750	1750	1800
L_{fix3} **(mm)**	2400	2400	2400	2200	2200	2450	2250	2300	2300	2200

Table A.12: von Mises stresses of model 22 and its derivatives

Stress location	Design Alternatives									
	22	**44**	**45**	**46**	**47**	**48**	**49**	**50**	**51**	**52**
Mass(kg)	1440	1460	1397	1397	1464	1460	1463	1455	1472	1462
1 (MPa)	153	150	149	141	142	152	143	149	149	142
2 (MPa)	152	137	151	146	134	140	136	143	141	134
3 (MPa)	136	122	136	143	127	125	127	124	116	127
4 (MPa)	115	115	117	104	103	108	108	108	120	106
5 (MPa)	169	169	172	155	153	160	160	161	175	157
6 (MPa)	154	154	156	143	141	147	147	147	158	145
7 (MPa)	152	152	151	142	143	154	144	151	150	143
8 (MPa)	167	151	166	166	150	151	148	158	146	149
9 (MPa)	137	124	137	132	124	124	124	123	121	124
10 (MPa)	133	133	135	117	115	123	123	123	139	120
11 (MPa)	118	103	111	109	100	102	100	103	109	100
12 (MPa)	136	133	153	149	130	131	129	132	136	130
13 (MPa)	132	130	150	147	126	128	127	128	128	127
14 (MPa)	168	166	184	175	163	162	162	163	165	162
15 (MPa)	139	136	161	160	134	136	135	136	132	135
16 (MPa)	142	142	139	142	144	142	144	142	140	145
17 (MPa)	135	135	133	141	143	139	139	139	132	141
18 (MPa)	150	133	144	143	131	133	130	135	132	132
19 (MPa)	126	113	126	124	112	114	113	114	112	112
20 (MPa)	149	146	145	137	138	149	138	145	148	138
21 (MPa)	141	123	135	141	128	119	130	128	116	128
22 (MPa)	142	127	142	141	126	129	119	130	128	124

Table A.13: Other alternatives_1

Parameters	**Design Alternatives**									
	1	**53**	**54**	**55**	**56**	**57**	**58**	**59**	**60**	**61**
α_1 **(Degree)**	2.62	2.62	1.49	3.18	1.13	3.18	3.18	3.18	3.18	3.18
α_2 **(Degree)**	3	3	4.08	3.47	5.02	3.47	3.47	3.47	3.70	3.70
α_3 **(Degree)**	5.72	6.5	7.89	10.73	10.73	10.73	10.73	10.73	9.80	9.40
α_4 **(Degree)**	5.66	4.5	2.5	3.30	3.04	2.70	2.20	2.20	2.40	2.80
R_1 **(mm)**	1200	1200	1002	1237	1172	1237	1237	1608	1650	1650
R_2 **(mm)**	2600	2600	1888	2048	1419	2048	2048	2470	2470	2470
L_1 **(mm)**	2830	2830	2830	2830	2830	2830	2830	2830	2830	2830
L_2 **(mm)**	1930	1930	1930	1930	1930	1930	1930	1930	1930	1930
L_3 **(mm)**	2550	2550	2550	2550	2550	2550	2550	2550	2550	2550
L_4 **(mm)**	1545	1545	1545	1545	1545	1545	1545	1545	1545	1545
t_1 **(mm)**	10	10	10	10	10	10	10	10	10	10
t_2 **(mm)**	15	15	15	15	15	15	15	15	15	15
t_3 **(mm)**	12	12	12	12	12	12	12	12	12	12
t_4 **(mm)**	12	12	12	12	12	12	12	12	12	12
t_5 **(mm)**	12	12	12	12	12	12	12	12	12	12
t_6 **(mm)**	12	12	12	12	12	12	12	12	12	12
t_7 **(mm)**	10	10	10	10	10	10	10	10	10	10
t_8 **(mm)**	15	15	15	15	15	15	15	15	15	15
L_{fix1} **(mm)**	2690	2690	2690	2690	2690	2690	2690	2690	2690	2690
L_{fix2} **(mm)**	1727	1727	1727	1727	1727	1727	1727	1727	1727	1727
L_{fix3} **(mm)**	2400	2400	2400	2400	2400	2400	2400	2400	2400	2400

Table A.14: von Mises stresses of Other alternatives_1

Stress location	**Design Alternatives**									
	1	**53**	**54**	**55**	**56**	**57**	**58**	**59**	**60**	**61**
Mass(kg)	1403	1406	1410	1465	1455	1460	1456	1443	1435	1433
1 (MPa)	162	161	155	151	145	151	151	151	149	148
2 (MPa)	171	174	144	155	135	151	148	161	158	159
3 (MPa)	155	156	192	158	196	160	162	154	155	155
4 (MPa)	126	123	116	88	90	90	91	95	102	103
5 (MPa)	178	178	176	150	152	152	154	160	166	167
6 (MPa)	161	162	158	136	138	138	140	145	150	151
7 (MPa)	161	161	154	150	144	150	150	150	148	148
8 (MPa)	181	180	159	158	150	158	158	160	156	158
9 (MPa)	153	154	171	149	179	149	150	149	150	150
10 (MPa)	144	140	133	100	101	102	104	117	121	122
11 (MPa)	135	136	166	136	171	138	139	134	135	135
12 (MPa)	150	151	149	138	143	140	140	142	143	141
13 (MPa)	148	146	147	114	128	116	117	122	128	129
14 (MPa)	186	187	185	137	147	140	142	151	158	159
15 (MPa)	159	157	161	121	140	124	125	131	138	140
16 (MPa)	147	145	136	117	117	118	119	118	123	125
17 (MPa)	143	140	131	108	108	109	110	110	116	118
18 (MPa)	161	161	148	145	139	145	145	146	143	144
19 (MPa)	140	141	164	137	171	136	137	137	136	137
20 (MPa)	158	158	152	148	142	148	148	148	146	146
21 (MPa)	150	146	121	121	112	120	119	131	128	129
22 (MPa)	160	160	148	153	125	151	153	153	154	153

Table A.15: Other alternatives_2

Parameters	**Design Alternatives**									
	1	**62**	**63(present)**	**64(without mid. Stiff)**	**65**	**66**	**67**	**68**	**69**	**70**
α_1 **(Degree)**	2.62	3.18	2.637	3.18	2.2	2	2	2.62	2.5	2.7
α_2 **(Degree)**	3	3.70	3.736	3.70	4	4	3.8	3.6	3.5	3.5
α_3 **(Degree)**	5.72	9.40	6.354	9.40	9.40	9.40	9.8	9.8	9.8	9.8
α_4 **(Degree)**	5.66	2.80	6.211	2.80	2.80	3	2.8	2.8	3.4	3.6
R_1 **(mm)**	1200	1650	1207.5	1650	1200	1400	1200	1400	1800	1800
R_2 **(mm)**	2600	2470	2607	2470	2490	2500	2535	2500	2720	2760
L_1 **(mm)**	2830	2900	2755	2900	2900	2900	2900	2900	2900	2900
L_2 **(mm)**	1930	1700	1800	1700	1700	1700	1700	1700	1700	1700
L_3 **(mm)**	2550	2380	2558	2380	2380	2380	2380	2380	2380	2380
L_4 **(mm)**	1545	1600	1595	1600	1600	1600	1600	1600	1600	1600
t_1 **(mm)**	10	10	10	10	10	10	10	10	10	10
t_2 **(mm)**	15	15	15	15	15	15	15	15	15	15
t_3 **(mm)**	12	12	12	12	12	12	12	12	12	12
t_4 **(mm)**	12	12	12	12	12	12	12	12	12	12
t_5 **(mm)**	12	15	16	15	15	15	15	15	15	15
t_6 **(mm)**	12	12	12	12	12	12	12	12	12	12
t_7 **(mm)**	10	10	10	10	10	10	10	10	10	10
t_8 **(mm)**	15	15	15	15	15	15	15	15	15	15
L_{fix1} **(mm)**	2690	2800	2658	2800	2800	2800	2800	2800	2800	2800
L_{fix2} **(mm)**	1727	1800	1495	1800	1800	1800	1800	1800	1800	1800
L_{fix3} **(mm)**	2400	2200	2458	2200	2200	2200	2200	2200	2200	2200

Table A.16: von Mises stresses of other alternatives_2

Stress location	**Design Alternatives**									
	1	**62**	**63**	**64**	**65**	**66**	**67**	**68**	**69**	**70**
Mass(kg)	140 3	1454	1445	1446	1465	1455	1464	1461	1445	1451
1 (MPa)	162	139	151	138	141	142	145	143	145	144
2 (MPa)	171	139	144	145	138	140	143	143	143	141
3 (MPa)	155	144	139	154	143	147	144	143	146	143
4 (MPa)	126	90	111	89	90	90	88	87	86	86
5 (MPa)	178	145	159	143	145	145	142	142	145	143
6 (MPa)	161	133	146	131	133	132	130	130	133	132
7 (MPa)	161	140	153	138	142	143	145	144	146	145
8 (MPa)	181	144	143	143	145	147	150	150	156	153
9 (MPa)	153	136	141	152	135	139	138	136	141	138
10 (MPa)	144	101	124	100	102	105	98	98	96	101
11 (MPa)	135	114	111	120	113	117	115	114	117	114
12 (MPa)	150	135	133	133	132	134	132	134	136	136
13 (MPa)	148	125	134	125	121	125	120	121	126	124
14 (MPa)	186	151	168	153	155	157	152	158	149	147
15 (MPa)	159	141	145	141	136	141	134	136	142	139
16 (MPa)	147	134	145	136	135	134	134	134	129	129
17 (MPa)	143	128	142	130	128	128	126	126	124	124
18 (MPa)	161	130	129	133	130	132	135	135	138	136
19 (MPa)	140	124	136	145	123	126	126	124	127	125
20 (MPa)	158	135	148	133	137	138	140	139	141	140
21 (MPa)	150	117	115	118	118	122	123	123	126	122
22 (MPa)	160	136	116	118	134	140	138	139	140	138

Table A.17: Other alternatives_3

Parameters	Design Alternatives									
	62	**71**	**72**	**73**	**74**	**75**	**76(75')**	**77**	**78**	**79(77')**
α_1 **(Degree)**	3.18	2.7	2.9	3	2.8	2.7	2.7	2.5	2.3	2.5
α_2 **(Degree)**	3.70	3.8	3.8	3.6	4	4.1	4.1	4.2	4.3	4.2
α_3 **(Degree)**	9.40	10	10.2	10.4	10.4	10.5	10.5	10.7	10.8	10.7
α_4 **(Degree)**	2.80	2.6	2.4	2.2	2.2	2	2	1.9	1.8	1.9
R_1 **(mm)**	1650	1500	1600	1700	1600	1600	1600	1550	1550	1550
R_2 **(mm)**	2470	2490	2450	2450	2370	2300	2300	2270	2230	2270
L_1 **(mm)**	2900	2900	2900	2900	2900	2900	2900	2900	2900	2900
L_2 **(mm)**	1700	1700	1700	1700	1700	1700	1700	1700	1700	1700
L_3 **(mm)**	2380	2380	2380	2380	2380	2380	2380	2380	2380	2380
L_4 **(mm)**	1600	1600	1600	1600	1600	1600	1600	1600	1600	1600
t_1 **(mm)**	10	10	10	10	10	10	10	10	10	10
t_2 **(mm)**	15	15	15	15	15	15	15	15	15	15
t_3 **(mm)**	12	12	12	12	12	12	12	12	12	12
t_4 **(mm)**	12	12	12	12	12	12	12	12	12	12
t_5 **(mm)**	15	15	15	15	15	15	15	15	15	18
t_6 **(mm)**	12	12	12	12	12	12	12	12	12	12
t_7 **(mm)**	10	10	10	10	10	10	10	10	10	10
t_8 **(mm)**	15	15	15	15	15	15	15	15	15	15
L_{fix1} **(mm)**	2800	2800	2800	2800	2800	2800	2800	2800	2800	2800
L_{fix2} **(mm)**	1800	1800	1800	1800	1800	1800	1800	1800	1800	1800
L_{fix3} **(mm)**	2200	2200	2200	2200	2200	2200	2200	2200	2200	2200

Table A.18: von Mises stresses of other alternatives_3

Stress location	Design Alternatives									
	62	**71**	**72**	**73**	**74**	**75**	**76(75')**	**77**	**78**	**79(77')**
Mass(kg)	1454	1463	1461	1455	1464	1463	1455	1466	1465	1482
1 (MPa)	139	140	139	141	138	137	136	137	137	122
2 (MPa)	139	139	137	141	133	129	130	127	123	121
3 (MPa)	144	143	144	147	146	149	157	149	151	131
4 (MPa)	90	86	84	84	84	85	84	83	81	151
5 (MPa)	145	141	141	141	140	141	138	139	139	219
6 (MPa)	133	130	129	130	129	129	127	128	128	191
7 (MPa)	140	141	140	142	138	138	136	138	138	120
8 (MPa)	144	146	143	146	140	138	136	137	137	110
9 (MPa)	136	135	135	139	136	138	155	139	141	138
10 (MPa)	101	97	96	94	95	99	98	93	93	183
11 (MPa)	114	113	114	117	116	118	123	119	121	138
12 (MPa)	135	135	135	138	135	135	133	134	134	124
13 (MPa)	125	121	121	123	121	121	121	120	121	97
14 (MPa)	151	148	146	147	145	146	148	144	144	91
15 (MPa)	141	136	136	138	136	137	137	136	137	109
16 (MPa)	134	133	129	128	129	129	131	127	125	133
17 (MPa)	128	125	124	122	122	122	124	120	120	103
18 (MPa)	130	131	129	131	126	125	122	124	124	95
19 (MPa)	124	123	123	126	125	127	148	127	129	131
20 (MPa)	135	136	135	137	134	129	132	133	133	116
21 (MPa)	117	120	117	120	111	107	109	105	103	99
22 (MPa)	136	136	135	146	134	132	116	128	131	112

Table A.19: Other alternatives_4

Parameters	Design Alternatives									
	77	**80**	**81**	**82(77)**	**83(77)**	**84(77)**	**85**	**86**	**87(77)**	**88**
α_1 **(Degree)**	2.5	2.5	2.3	2.5	2.5	2.5	2.5	2.5	2.5	2.2
α_2 **(Degree)**	4.2	4	4.2	4.2	4.2	4.2	4.2	4.3	4.3	4.3
α_3 **(Degree)**	10.7	10.7	10.7	10.7	10.7	10.7	10.7	10.7	10.7	5
α_4 **(Degree)**	1.9	2.1	2.1	1.9	1.9	1.9	2	1.9	1.9	7.1
R_1 **(mm)**	1550	1550	1550	1550	1550	1550	1550	1550	1550	1200
R_2 **(mm)**	2270	2350	2310	2270	2270	2270	2290	2240	2240	2750
L_1 **(mm)**	2900	2900	2900	2820	2900	2900	2900	2900	2900	2900
L_2 **(mm)**	1700	1700	1700	1820	1700	1700	1700	1700	1700	1700
L_3 **(mm)**	2380	2380	2380	2500	2500	2500	2500	2500	2500	2500
L_4 **(mm)**	1600	1600	1600	1600	1670	1600	1600	1600	1600	1600
t_1 **(mm)**	10	10	10	10	10	10	10	10	10	10
t_2 **(mm)**	15	15	15	15	15	15	15	15	15	15
t_3 **(mm)**	12	12	12	12	12	12	12	12	12	12
t_4 **(mm)**	12	12	12	12	12	12	12	12	12	12
t_5 **(mm)**	15	15	15	15	15	15	15	15	15	15
t_6 **(mm)**	12	12	12	12	12	12	12	12	12	12
t_7 **(mm)**	10	10	10	10	10	10	10	10	10	10
t_8 **(mm)**	15	15	15	15	15	15	15	15	15	15
L_{fix1} **(mm)**	2800	2800	2800	2900	2880	3000	3000	3000	3200	3000
L_{fix2} **(mm)**	1800	1800	1800	1800	1800	1800	1800	1800	1800	1800
L_{fix3} **(mm)**	2200	2200	2200	2200	2200	2200	2200	2200	2200	2200

Table A.20: von Mises stresses of other alternatives_4

Stress location	Design Alternatives									
	77	**80**	**81**	**82(77)**	**83(77)**	**84(77)**	**85**	**86**	**87(86)**	**88**
Mass(kg)	1466	1464	1465	1460	1458	1458	1459	1459	1456	1438
1 (MPa)	137	139	138	138	137	137	137	136	136	138
2 (MPa)	127	134	130	126	127	127	128	125	125	131
3 (MPa)	149	148	150	147	150	150	149	150	150	136
4 (MPa)	83	82	82	90	83	83	83	84	84	116
5 (MPa)	139	139	139	152	139	139	139	139	139	161
6 (MPa)	128	128	128	139	128	128	128	128	128	149
7 (MPa)	138	140	139	139	138	138	138	137	137	139
8 (MPa)	137	141	139	138	138	138	139	137	138	147
9 (MPa)	139	137	138	136	139	139	138	139	139	129
10 (MPa)	93	92	92	104	93	93	93	98	98	128
11 (MPa)	119	118	119	121	119	119	118	119	119	107
12 (MPa)	134	134	133	136	134	134	133	133	133	132
13 (MPa)	120	120	121	123	121	121	120	120	120	141
14 (MPa)	144	143	143	149	149	144	143	144	144	177
15 (MPa)	136	135	136	135	136	136	135	136	136	152
16 (MPa)	127	127	127	121	127	127	127	128	128	154
17 (MPa)	120	120	120	115	120	120	120	120	120	153
18 (MPa)	124	127	126	125	125	125	125	124	125	130
19 (MPa)	127	127	128	126	127	127	127	127	127	118
20 (MPa)	133	135	134	134	133	133	133	132	132	134
21 (MPa)	105	111	107	103	105	105	106	103	103	120
22 (MPa)	128	137	134	129	129	129	134	129	129	129

Table A.21: Other alternatives_5

Parameters	Design Alternatives				
	74	**89**	**95**	**96**	**97**
α_1 **(Degree)**	2.8	2.8	2.57	2.8	2.8
α_2 **(Degree)**	4	4	3.8	4.1	4.1
α_3 **(Degree)**	10.4	10.4	10.376	10.4	10.4
α_4 **(Degree)**	2.2	2.2		5.66	6.21
R_1 **(mm)**	1600	1600	1557.5	1600	1600
R_2 **(mm)**	2370	2370	2307.5	2350	2350
L_1 **(mm)**	2900	2900	2900	2900	2900
L_2 **(mm)**	1700	1700	1705	1700	1700
L_3 **(mm)**	2380	2500	2500	2500	2500
L_4 **(mm)**	1600	1600	1600	1600	1600
t_1 **(mm)**	10	10	10	10	10
t_2 **(mm)**	15	15	15	15	15
t_3 **(mm)**	12	12	12	12	12
t_4 **(mm)**	12	12	12	12	12
t_5 **(mm)**	15	15	15	15	15
t_6 **(mm)**	12	12	12	12	12
t_7 **(mm)**	10	10	10	10	10
t_8 **(mm)**	15	15	15	15	15
L_{fix1} **(mm)**	2800	3200	2700	3200	3200
L_{fix2} **(mm)**	1800	1800	1300	1800	1800
L_{fix3} **(mm)**	2200	2200	2200	2200	2200

Table A.22: von Mises stresses of other alternatives_5

Stress location	Design Alternatives									
	74	**89**	**90**	**91(90')**	**92(90'')**	**93**	**94(90''')**	**95**	**96**	**97**
Mass(kg)	1464	1452	1454	1445	1509	1431	1453	1458	1482	1487
1 (MPa)	138	138	137	136	136	152	149	141	137	137
2 (MPa)	133	134	131	146	136	147	137	137	138	142
3 (MPa)	146	146	146	156	142	145	151	151	137	135
4 (MPa)	84	84	84	84	83	111	85	85	77	76
5 (MPa)	140	140	140	138	136	159	139	139	129	127
6 (MPa)	129	129	129	127	125	146	128	128	120	118
7 (MPa)	138	139	138	136	137	154	150	142	138	138
8 (MPa)	140	142	140	138	126	156	143	143	146	153
9 (MPa)	136	136	135	153	136	147	140	140	131	130
10 (MPa)	95	95	95	94	92	124	94	94	83	82
11 (MPa)	116	116	116	121	111	116	121	121	109	107
12 (MPa)	135	134	134	131	117	138	138	138	128	127
13 (MPa)	121	121	121	120	106	134	122	122	112	110
14 (MPa)	145	145	145	148	138	168	145	145	130	128
15 (MPa)	136	136	136	136	118	144	138	138	124	122
16 (MPa)	129	129	129	131	133	144	129	129	126	125
17 (MPa)	122	122	122	124	126	132	122	122	117	116
18 (MPa)	126	127	126	124	115	138	129	129	131	132
19 (MPa)	125	125	125	146	130	142	129	129	120	119
20 (MPa)	134	134	133	131	132	149	145	137	133	133
21 (MPa)	111	112	109	111	101	127	114	115	118	127
22 (MPa)	134	135	130	116	104	120	138	138	133	130

REFERENCES

[1] H. Ugail, M.J. Wilson, Efficient shape parametrisation for automatic design optimisation using a partial differential equation formulation, Computers and Structures 81, pp 2601-2609, 2003

[2] D.Holm, M. MackAldener, H. Hellman, Structural optimization in industrial applications, Welded High-Strength Steel Structures, EMAS,1997

[3] Joong Jae Kim, Heon Young Kim, Shape design of an engine mount by a method of parameter optimization, Computer & Structures Vol. 65, No. 5, pp 725-731, 1997

[4] Jyhwen Wang, Design optimization of rigid metal containers, Finite Elemets in Analysis and Design 37, pp 273-286, 2001

[5] Edwin Hardee, Kuang-Hua Chang, Jian Tu, Kyung K. Choi, Iulian Grindeanu, Xiaoming, A CAD-based design parameterization for shape optimization of elastic solids, Advances in Engineering Software 30,pp 185-199, 1999

[6] Pasi Tanskanen, The evolutionary structural optimization method: theoretical aspects, Comput. Methods Appl. Mech. Engrg. 191, pp 5485-5498, 2002

[7] Y.M. Xie, G.P. Steven, A simple evolutionary procedure for structural optimization, Computer and Structure 49, pp 885-896, 1993

[8] R. Das, R. Jones and Y.M. Xie, Design of structures for optimal static strength using ESO, Engineering Failure Analysis 12, pp 61-80, 2005

[9] Baolin Wan, Dimitris C. Rizos, Michael F. Petrou, Kent.A. Harries, Computer simulations and parametric studies of GFRP bridge deck system, Composite Structure 69, pp 103-115, 2005

[10] L. Gil, A. Andreu, Shape and cross-section optimisation of a truss structure, Computer and Structure 79, pp 681-689, 2001

[11] K.-H. Chang, P.-S. Tang, Integration of design and manufacturing for structural shape optimisation, Advances in Engineering Software 32, pp 555-567, 2001

[12] A.E. Tekkaya, A. Güneri, Shape optimization with the biological growth method: a parameter study, Computer-aided Engineering and Software, vol. 13 No. 8, pp 4-18, 1996

[13] Q. Li, G.P. Steven, O.M. Querin, Y.M. Xie, Evolutionary shape optimization for stress minimization, Mechanism Research Communication, Vol. 26, No. 6, pp 657-664, 1999

[14] D.T.Pham, D. Karaboğa, Intelligent Optimisation Techniques, Springer-Verlag London Limited 2000, 2nd Printing 2000

[15] T. Toprak, E. Bozdağ, E. Sümbüloğlu, Hidromek- HMK 220 LC Ekskavatör bomunun dinamik gerilme analizi, Temmuz 2003

[16] John E. Pearson, W. Robert Hannen and Erik Soderberg, Development of Fatigue Monitoring System for a Hydraulic Excavator, Practice periodical on structural design and construction, November 2004.

[17] Hsin-Sheng Lee, Shinn-Liang Chang and Kuo-Huang Lin, A study of the design, manufacture and remote control of a pneumatic excavator, International Journal of Mechanical Engineering Education, 32/4

[18] Johan Martinsson, Fatigue Assessment of Complex Welded Steel Structures, Doctoral Thesis, Division of Lightweight structures at Department of Aeronautical and Vehicle Engineering at the Royal Institute of Technology, Stockholm, 2004

[19] Sang Hoon Lee and Byung Man Kwak, A Versatile Structural Optimisation System Based on the Taguchi Method, ICES 2002, http://khp.kaist.ac.kr/.

[20] Mehmet Yener, Ferhan Fıçıcı, Eres Söylemez, Timur Arıkoğlu, İş makinaları konstrüksiyonlarının tasarımında bilgisayar ortamında sonlu eleman analizi metoduyla mukavemet analizlerinin yapılması ve önemi, İş makinaları sempozyumu bildiri kitapçığı, 2003.

[21] Goldberg, D.E (1989): Genetic Algorithms in Search, Optimisation and machine Learning. Addison-Wesley Publishing Co., Reading, Massachusetts.

[22] Osyczka A. (2002): Evolutionary algorithms for single and multicriteria design optimization; with 24 tables, Heidelberg; New York: Physica-Verl.

[23] Ehrgott, M. (1997): Multiple Criteria Optimisation- Classification and Methodology, Shaker Verlag, Aachen.

[24] Lin,S., Kernighan, B. W., "An effective Heuristic Algorithm for the traveling Salesman Problem", Operations Research, Vol. 21, No.2, March-April 1973, pp 498-516

[25] Kernighan, B. W., Lin,S., "An effective Heuristic Procedure for Partitioning Graphs", The Bell Systems Tech. Journal, Vol.49, No. 2, Feb. 1970, pp 291-307.

[26] Dote Y. (1990), Fuzzy and neural network controller, 16th Annual Conf. IEEE Industrial Electronics Society Pacific, Grove, CA, Vol.2, pp 1314-1343.

[27] Gupta, M.M., Kiszka, J.B. and Trojan, G.M. (1986) Fusion of fuzzy logic and neural networks with applications to decision and control problems, Proc. American Control Conference, Vol.1, pp 30-31.

[28] SAE J1179, Hydraulic excavator and backhoe digging forces, SAE Handbook volume 3, 1995, 40.355

[29] E. A. Avallone, T. Baumaister iii, Marks' Standard Handbook for Mechanical Engineers 10th edition, McGRAW-HILL International editions, pp 10.26

[30] Phadke, M. S (1989) : Quality Engineering Using Robust Design, Prentice Hall, New Jersy.